

RESEARCH ARTICLE

PH20 is not expressed in murine CNS and oligodendrocyte precursor cells

Mathieu Marella¹, Joe Ouyang¹, Jonathan Zombeck², Chunmei Zhao¹, Lei Huang¹, Robert J. Connor¹, Kim B. Phan¹, Michael C. Jorge¹, Marie A. Printz¹, Rudolph D. Paladini¹, Arnold B. Gelb¹, Zhongdong Huang¹, Gregory I. Frost¹, Barry J. Sugarman¹, Lawrence Steinman³, Ge Wei¹, H. Michael Shepard¹, Daniel C. Maneval¹ & Paula J. Lapinskas¹

¹Halozyne Therapeutics, Inc., San Diego, California

²Biomodels LLC, Watertown, Massachusetts

³University School of Medicine, Department of Neurology and Neurological Sciences, Beckman Center for Molecular Medicine, Stanford University, Stanford, California

Correspondence

Daniel C. Maneval, Halozyne Therapeutics, Inc., 11388 Sorrento Valley Road, San Diego, CA 92121. Tel: 1-858-704-8148; Fax: 1-858-704-8300; E-mail: dmaneval@halozyne.com

Funding Information

The authors also acknowledge financial support from Baxter International.

Received: 18 January 2016; Revised: 8 December 2016; Accepted: 10 January 2017

Annals of Clinical and Translational Neurology 2017; 4(3): 191–211

doi: 10.1002/acn3.393

Abstract

Objective: Expression of *Spam1*/PH20 and its modulation of high/low molecular weight hyaluronan substrate have been proposed to play an important role in murine oligodendrocyte precursor cell (OPC) maturation in vitro and in normal and demyelinated central nervous system (CNS). We reexamined this using highly purified PH20. **Methods:** Steady-state expression of mRNA in OPCs was evaluated by quantitative polymerase chain reaction; the role of PH20 in bovine testicular hyaluronidase (BTH) inhibition of OPC differentiation was explored by comparing BTH to a purified recombinant human PH20 (rHuPH20). Contaminants in commercial BTH were identified and their impact on OPC differentiation characterized. *Spam1*/PH20 expression in normal and demyelinated mouse CNS tissue was investigated using deep RNA sequencing and immunohistological methods with two antibodies directed against recombinant murine PH20. **Results:** BTH, but not rHuPH20, inhibited OPC differentiation in vitro. Basic fibroblast growth factor (bFGF) was identified as a significant contaminant in BTH, and bFGF immunodepletion reversed the inhibitory effects of BTH on OPC differentiation. *Spam1* mRNA was undetected in OPCs in vitro and in vivo; PH20 immunolabeling was undetected in normal and demyelinated CNS. **Interpretation:** We were unable to detect *Spam1*/PH20 expression in OPCs or in normal or demyelinated CNS using the most sensitive methods currently available. Further, “BTH” effects on OPC differentiation are not due to PH20, but may be attributable to contaminating bFGF. Our data suggest that caution be exercised when using some commercially available hyaluronidases, and reports of *Spam1*/PH20 morphogenic activity in the CNS may be due to contaminants in reagents.

Introduction

PH20, a glycosylphosphatidylinositol-anchored hyaluronidase encoded by the Sperm Adhesion Molecule 1 (*Spam1*) gene,^{1–3} is expressed in the adult male reproductive tract. This enzyme plays a nonessential role in sperm penetration of the hyaluronan (HA)-rich cumulus of oocytes during fertilization.^{4–7} *Spam1*/PH20 expression in adult testis and epididymis has been well documented.^{8–10} The

literature also contains unconfirmed reports of *Spam1* gene expression in other tissues, such as the female reproductive tract,¹¹ kidney,¹² breast,¹³ and synovium/chondrocytes,¹⁴ and in multiple tumor types.^{13,15}

Recently, *Spam1*/PH20 expression was reported in murine oligodendrocyte precursor cells (OPC) in vitro, in normal adult mouse brain, in OPCs in demyelinating spinal cord lesions of an experimental autoimmune encephalomyelitis (EAE) mouse model, in chronic cortical

Table 1. Key cell culture media and supplements.

Reagent	Source	Components
NeuroCult Basal Medium	STEMCELL Technologies	Basal media
NeuroCult Proliferation Supplement	STEMCELL Technologies	Basal media
Complete NSC Proliferation Medium	STEMCELL Technologies	NeuroCult Basal Medium NeuroCult proliferation supplement Before use, add 20 ng/mL human EGF and bFGF (final concentration)
Oligodendrocyte precursor cell proliferation medium (OPCPM)	STEMCELL Technologies	DMEM/F12 (Life Technologies) N1 medium supplement B27 minus Vitamin A 10 μ mol/L D-Biotin 10% BSA Before use, add 20 ng/mL of human bFGF and PDGF α
Oligodendrocyte precursor cell differentiation medium (OPCDM)	STEMCELL Technologies	DMEM/F12 (Life Technologies) Pen Strep 10% BSA 5 μ L of 3 mmol/L T3 500 μ L of 5 mg/mL NAC
Recombinant Human EGF	PreproTech (Oak Park, CA)	Specific media additive (for NSC Proliferation Medium)
Recombinant Human FGF basic	PreproTech	Specific media additions (NSC Proliferation Medium and OPCPM)
Recombinant Human PDGF α	PreproTech	Specific media supplement (OPCPM)
T3	Sigma-Aldrich	Specific media supplement (OPCPM)
N1	Sigma-Aldrich	Specific media supplement (OPCPM)
D-Biotin	Sigma-Aldrich	Specific media supplement (OPCPM)
NAC	Sigma-Aldrich	Specific media supplement (OPCPM)
B27 minus Vitamin A	Life Technologies	Specific media supplement (OPCPM)

BSA, bovine serum albumin; DMEM, Dulbecco's modified Eagle's medium; EGF, epidermal growth factor; FGF, fibroblast growth factor (also known as bFGF, basic fibroblast growth factor); NAC, N-acetyl-L-cysteine; NSC, neural stem cell; PDGF α , platelet-derived growth factor subunit alpha polypeptide; T3, triiodothyronine.

lesions of multiple sclerosis (MS) patients, and in white matter injury in fetal sheep brain.^{16,17} These reports hypothesized that elevated PH20 expression in demyelinating lesions promotes accumulation of PH20-specific HA degradation products that inhibits OPC differentiation and results in reduced remyelination. Hyaluronan does have many different functions, including a structural role in brain perineural nets.¹⁸ If PH20 is expressed during OPC regeneration and alters neural function, this would be a very important finding. For this reason, we endeavored to confirm some of the findings in the original reports.^{16,17}

The following studies were conducted: (1) characterization of *Spam1* mRNA expression by reverse transcription quantitative polymerase chain reaction (RT-qPCR) in primary murine neuronal and glial cells; (2) exploration of the role of PH20 in OPC differentiation by comparing recombinant human PH20 (rHuPH20) and commercial bovine testicular hyaluronidases (BTH); (3) determination of the purity of BTH IV-S; and (4) characterization of *Spam1*/PH20 expression in the brain and spinal cord of normal adult and EAE mouse models.^{19,20}

Methods

Primary murine cell culture

Commercially available primary OPCs, derived from cryopreserved mouse cortical neurospheres isolated on embryonic day 14, were cultured according to manufacturer's instructions (STEMCELL Technologies, Vancouver, BC, Canada). OPCs were generated from neurospheres plated in an eight-well chamber slide in OPC proliferation medium (OPCPM). OPCs were further differentiated to oligodendrocytes (OL) in OPC differentiation media (OPCDM) per manufacturer's instructions and were used to evaluate the effect of treatments on OPC differentiation. For details of components of cell culture reagents, see Table 1. Cells were cultured in eight-well chamber slides (triplicate wells per treatment), and the OPC differentiation to mature myelinating OLs was detected by immunofluorescence detection using a mouse antibody to myelin basic protein (SMI 94; anti-HuMBP which cross-reacts with mouse; Covance, Princeton, NJ). Primary astrocytes and cortical neurons were cultured in appropriate cell culture media according to

manufacturer's instructions (ScienCell Research Laboratories, Carlsbad, CA) and served as controls for determining neuronal and glial cell origin.

OPC culture treatments

Reagents used in OPC differentiation studies are listed in Table 2, and the specific PH20 hyaluronidase preparations are listed in Table 3. Prior reports have compared the enzymatic activity of BTH and rHuPH20 and provide more detailed information on the purity and characteristics of both enzymes.^{21,22} Both bFGF and BTH IV-S (Sigma-Aldrich, St. Louis, MO) were inactivated by heating to 95–100°C for 30 min. Immunodepletion of bFGF from BTH IV-S was performed by immunoprecipitation using a mouse anti-bFGF neutralizing antibody (anti-FGF2, EMD Millipore, Billerica, MA) and Protein A/G Plus resins column purification (Pierce, Thermo Fisher Scientific, Rockford, IL). bFGF depletion was confirmed by western blot probing with a primary anti-FGF2 antibody (EMD Millipore) followed by a goat anti-mouse horseradish peroxidase (HRP) secondary antibody (EMD Millipore) and visualized by enhanced chemiluminescence (ECL; GE Healthcare, Pittsburgh, PA). Effects of a pan-FGF receptor inhibitor, PD173074 (Sigma-Aldrich), were evaluated in combination with BTH VI-S and bFGF treatment.

OPC immunofluorescence labeling and analysis

To determine differentiation of OPCs to mature myelin-producing OLs, cells were incubated in OPCDM with or without treatments for 48–96 h, and then fixed with 4% paraformaldehyde in phosphate-buffered saline (PBS). Following blocking and washing of cells, the slides were incubated with a mouse monoclonal anti-MBP antibody (Covance Research Products, Cumberland, VA), counterstained with 4', 6-diamidino-2-phenylindole (DAPI) at 4°C overnight to visualize nuclei, and incubated with Alexa Fluor 488- or Alexa Fluor 594-conjugated donkey secondary antibodies (Jackson ImmunoResearch, West Grove, PA). Slides were mounted with ProLong Gold

Table 2. Treatments.

Reagent	Source	Concentration
Oligodendrocyte precursor cell differentiation medium (control)	STEMCELL Technologies	Not applicable
Bovine basic fibroblast growth factor (bFGF)	R&D Systems	10 ng/mL
Bovine bFGF, heat inactivated	R&D Systems	10 ng/mL
PD173074	Sigma-Aldrich	10 nmol/L

Antifade with DAPI medium (Life Technologies, Carlsbad, CA) and photomicrographs were captured with an Axioskop microscope (Carl Zeiss Microscopy, Oberkochen, Germany) or Eclipse TE2000-U inverted microscope (Nikon, Tokyo, Japan). Mouse immunoglobulin G (IgG) was used as a negative control. MBP-positive cells were counted using a fluorescence microscope (Carl Zeiss) with a manual cell counter and compared to control (OPCDM). Results were reported as percent (%) of control MBP-positive cells.

Determination of HA in culture medium and oligodendrocytes

A commercial HA enzyme-linked immunosorbent assay (ELISA) kit (DuoSet ELISA System1: Hyaluronan, R&D Systems, Minneapolis, MN) was used to quantify HA levels in cell culture supernatants. To visualize levels of HA produced by OPCs, cells were cultured in OPCDM and incubated with a biotinylated HABP (bHABP; Seikagaku Kogyo Co., Tokyo, Japan); the HABP complex was detected with Alexa Fluor 488-conjugated Streptavidin (Jackson ImmunoResearch).

Statistical analysis of OPC studies

Statistical significance between the means of the treatment groups was evaluated by one-way analysis of variance (ANOVA) using GraphPad Prism v6.0 (GraphPad Software, La Jolla, CA). DAPI-positive cells were counted using an inverted immunofluorescence microscope (Nikon) with MetaMorph image analysis software v7.8.2 (Molecular Devices, Sunnyvale, CA).

Proteins present in BTH preparations and rHuPH20 by SDS-PAGE gel electrophoresis

BTH IV-S, BTH VI-S, and rHuPH20 (12 µg each) were resolved by electrophoresis in a 4–20% Criterion TGXTM

Table 3. Hyaluronidases.

Reagent	Source	Concentration (µg/mL)	Specific activity (U/mg)
rHuPH20	Halozyme Therapeutics, Inc.	10.0	122,176
BTH VI-S	Sigma-Aldrich	20.0	3689
BTH IV-S	Sigma-Aldrich	40.0	1,421
BTH IV-S (heat inactivated)	Sigma-Aldrich	22.5	<60
BTH IV-S (bFGF depleted)	Sigma-Aldrich	22.5	Not available

BFGF, basic fibroblast growth factor; BTH, bovine testicular hyaluronidase; rHuPH20, recombinant human PH20.

gel (Bio-Rad Life Sciences, Hercules, CA) using Tris-Glycine SDS running buffer (Invitrogen, Carlsbad, CA). Proteins were visualized by staining with the Coomassie-based dye InstantBlue (Expedeon, San Diego, CA). Molecular weight standards (15–150 kDa) were included to approximate protein size.

Analysis of BTH IV-S by multi-analyte profiling

BTH IV-S (Sigma) was analyzed using multiplexed immunoassays with the RodentMAP v3.0 platform (Myriad RBM, Austin, TX). Because the sequences of bovine and murine bFGF are 94.8% homologous, and because western blot analyses demonstrated that the anti-murine bFGF antibody used in the RodentMAP v3.0 kit could detect bovine bFGF, the RodentMAP v3.0 was qualified for its intended use.

Quantitation of bFGF/FGF2 in commercial hyaluronidase preparations

Concentrations of bFGF in BTH IV-S and BTH VI-S (Sigma) were determined using the Human FGF basic Quantikine ELISA kit following manufacturer's instructions (R&D Systems). A correction factor was used to calibrate the assay for bovine versus human bFGF.

Isolation of RNA

Total RNA was isolated from primary OPCs, astrocytes, cortical neuron cells, and testis of adult C57BL/6 mouse using the Trizol reagent (Life Technologies, Grand Island, NY) in Lysing Matrix D tubes (MP Biomedical, Santa Ana, CA) and homogenized using a Fast Prep-24 (MP Biomedical) according to manufacturer's instructions. Isolated RNA was treated with 10 U RNase-free DNase I (New England Biolabs, Ipswich, MA), then purified using the RNeasy MinElute Cleanup Kit (Qiagen, Germantown, MD) per manufacturer's instructions. RNA purity was determined using a NanoDrop 2000 Spectrophotometer (Thermo-Scientific, Waltham, MA). Integrity was confirmed by agarose gel electrophoresis. Complementary DNA (cDNA) was prepared from 1.0 μ g of each RNA sample using oligo (dT) primers and the Superscript III First-Strand Synthesis System for RT-qPCR (Invitrogen) according to manufacturer's instructions.

Tissues from control and EAE mice were used to isolate RNA for deep RNA sequencing. Spinal cord and corpus callosum enriched for dentate gyrus were dissected on ice, then snap frozen in liquid nitrogen. To enrich for dentate gyrus, the whole brain (maintained on ice) was bifurcated along the longitudinal fissure, and the corpus

callosum was excised from one hemisphere. The spinal cord was excised by spinal level, and focus was placed on lumbar spinal cord sections. Tissues (~100 mg) were then placed in Lysing Matrix D tubes, snap frozen in liquid nitrogen, and stored in a -80°C freezer until used for deep RNA sequencing.

RT-qPCR analysis

All RT-qPCR reactions were carried out using the Applied Biosystems ViiA 7 Real Time PCR System (Applied Biosystems, Foster City, CA) and specific primer/probe sets designed to run in Taqman Fast Advanced Master Mix (Applied Biosystems) with template cDNA, equivalent to 50 ng original input RNA. Validated primer/probe sets for murine *Spam1*, *β -actin*, Doublecortin (*Dcx*), Platelet-Derived Growth Factor Receptor-alpha (*PDGFR α*), and Neuronal nuclei (*NeuN*), designed to span intron (i.e., exon-specific) were purchased from Applied Biosystems. The fidelity of the murine *Spam1* primer/probe set was verified by sequencing the 124 base pair amplicon product that was generated using murine testis cDNA as a template in the RT-qPCR reaction as a positive control. The PCR efficiencies of the *Spam1* and *β -actin* reactions were 99% or greater.

Deep RNA sequencing library construction and analysis

RNA concentrations were determined using a fluorimetric Quant-iT RNA assay (Invitrogen) and RNA Integrity Number values were determined using TapeStation (Agilent, Santa Clara, CA).

RNA was converted into a cDNA library using polyadenylated RNA bound to oligo-dT magnetic beads (Illumina, San Diego, CA; performed by Beckman Coulter Genomics, Danvers, MA). Library suitability was confirmed for high-throughput DNA sequencing and for subsequent cluster generation using TruSeq RNA Sample Prep Kit v2 (Illumina; performed by Beckman Coulter Genomics) according to manufacturer's instructions. The mRNA was fragmented enzymatically prior to first and second strand cDNA synthesis. The cDNA was end-repaired and ligated to Illumina adaptors. Adaptor-ligated cDNA was PCR-amplified 15 cycles, and purified using AMPure XP (Beckman Coulter Genomics).

Libraries were sequenced on a HiSeq 2500 instrument (Illumina) and multiplexed in sequencing lane 12-plexes with compatible libraries aiming for outputs of approximately 42 million bp paired-end reads. Sequencing performance met Illumina specifications. Quality scores and passing filter percentages were evaluated as well as overall data amounts generated (Beckman Coulter Genomics).

Following sequencing, the data were trimmed to 75 bp paired-end reads and de-multiplexed by index using Casava v1.8.2 (Illumina). One forward and one reverse fastq file for each sample was used for further expression analysis. The reads were aligned to the mouse transcriptome (Ensembl v74 genome release) and appended with synthetic External RNA Control Consortium (ERCC) sequences, which were spiked into the library upon construction and used for normalization of all samples for differential expression analyses. Expression values are presented as fragments per kilobase of exon per million as calculated by Cufflinks v2.1.1, based upon sequence alignment by TopHat v2.09.

Directed query of the stanford multiple sclerosis proteome database

A directed query of the Stanford Multiple Sclerosis Proteome Database²³ was performed to assess PH20 protein expression. This database contains proteome data derived from a sensitive laser capture microdissection and proteomic analysis of acute plaques, chronic active plaques, and chronic plaques from six patients with confirmed MS, as well as control tissues from age-matched individuals whose brains were devoid of central nervous system (CNS) abnormalities. The samples isolated by laser capture microdissection were separately analyzed by nanoliquid chromatography and tandem mass spectrometry to determine their global protein expression profiles. To ascertain reliable protein identification, the criterion of stringent mass tolerance was used to eliminate false-positive proteins by searching against a forward and reverse human protein database.²⁴ To enhance maximal protein detection coverage, samples were analyzed 4–7 times by mass spectrometric analysis until a saturation point was reached. Mean spectral counts (SCs) ranged from 0 to 556; the smallest nonzero mean SC that could be discriminated was 0.3. The mean SCs were categorized into three groups to allow for semi-quantitative comparisons: ≤ 9.9 , 10.0–99.9, and ≥ 100 mean SC. Analysis yielded 2574 proteins with high confidence. The entire database is available in the Supplementary data in Han *et al.*²⁴ To the best of our knowledge, this is the largest and the most comprehensive proteome of MS brain lesions characterized to date.

EAE mouse model development

An EAE model induced with immunization with myelin oligodendrocyte glycoprotein (MOG) was induced in female C57BL/6J mice as previously described.^{19,20} Following induction of EAE, the whole brain and spinal cord were dissected from half of the mice of each group and processed for immunohistochemistry and the other half

for deep RNA sequencing. The protocol for the study was approved by Biomedel's Institutional Animal Care and Use Committees, and was conducted in accordance with the United States Public Health Service's Policy on Humane Care and Use of Laboratory Animals.

Immunohistochemical evaluation of PH20 protein expression in CNS of normal adult and EAE mice

The whole brain, lumbar spinal cord, and testis were harvested after transcardial perfusion of the mice with 4% paraformaldehyde. Harvested tissues were then post-fixed in formalin and embedded in paraffin blocks (FFPE). Five micrometer sections were mounted on glass slides, heated at 60°C for 1 h and stored at ambient temperature until use. For antibody labeling, heat-induced epitope retrieval (10 mmol/L TRIS, 1 mmol/L EDTA pH 8) were performed by microwave (700 W, 10% power, 10 min). To demonstrate selectivity of two rabbit polyclonal antibodies generated against a recombinant murine PH20 (rMuPH20), antibodies Ab2678 and Ab1637 (Halozyme Therapeutics, San Diego, CA) were incubated with 400 $\mu\text{g}/\text{mL}$ of rMuPH20 or recombinant murine Hyal5 proteins (Halozyme Therapeutics) for 90 min before staining. A pre-immune serum at the same dilution ratio was used to compare specificity of binding of the antibody preparation. Following washing, secondary antibody was applied on slides for 30 min (2 $\mu\text{g}/\text{mL}$ of biotin-goat anti-rabbit diluted in PBS containing 10% goat serum; Life Technologies). Antibody binding was visualized with Vectastain ABC Elite (Vector Laboratories, Burlingame, CA) according to manufacturer's instructions.

Staining of MuPH20 and myelin on sections of lumbar spinal cord and corpus callosum of control and EAE mice was evaluated using antibodies Ab2678 and Ab1637 raised against rMuPH20 or anti-MBP antibody (Covance). Briefly, FFPE sections of the spinal cord were deparaffinized in three changes of xylene and hydrated through a gradient of ethanol in distilled water (100%, 80%, 70%, 50%, 0%). Heat-induced epitope retrieval was used; slides were heated to 95°C in a citrate-buffered solution (pH 6) using a commercial microwave (700 W, 10% power, 10 min). Tissue sections were blocked in PBS containing 10% goat serum for 30 min. Subsequently, dilutions of primary antibodies in PBS containing 10% goat serum were incubated as follows: mouse monoclonal anti-MBP (Covance) 1/300, overnight at 4°C; rabbit polyclonal anti-rMuPH20 Ab1637 or Ab2678 (Halozyme Therapeutics) 2.5 $\mu\text{g}/\text{mL}$ overnight at 4°C or 30 min at ambient temperature, respectively. Secondary antibodies (Alexa Fluor 488 anti-mouse antibody and Alexa Fluor 594 anti-rabbit antibody, Jackson ImmunoResearch) were applied to

detect immunolabeling. Slides were mounted in Vectashield+DAPI mounting medium (Vector Laboratories). Representative photomicrographs were digitally captured using a Zeiss Axioskop microscope equipped with a SPOT Pursuit digital camera (Spot Imaging Solutions, Sterling Heights, MI).

Histolocalization of HA patterns in relationship to demyelination in spinal cord

Myelination and HA staining patterns were evaluated in transverse sections of lumbar spinal cord from control and EAE mice. HA labeling was detected using a probe consisting of a TSG-6 link module fused with the Fc backbone of human IgG1.²⁵ Myelin labeling was detected using a mouse monoclonal anti-MBP antibody. Binding protein or primary antibody was incubated overnight at 4°C in PBS containing 10% goat serum, and secondary antibodies (Alexa Fluor 488 streptavidin and Alexa Fluor 594 anti-mouse antibody, Jackson ImmunoResearch) were applied to detect bound complexes. Images were captured by an Axioskop microscope (Carl Zeiss) equipped with a Pursuit camera (Spot Imaging Solutions). Merged pseudocolored images of control and EAE spinal cord labeled with HTI-601 and anti-MBP were produced.

Production and characterization of polyclonal rabbit antibodies to rMuPH20

Two polyclonal rabbit antibodies directed against rMuPH20 were produced by subcutaneous (s.c.) dosing of New Zealand White rabbits with or without Freund's Adjuvant (Sigma-Aldrich). For Ab1637, the initial immunization consisted of s.c. injections of rMuPH20 alone. For Ab2678, the initial immunization consisted of four 100 μ L s.c. injections of a 1:1 mix of Complete Freund's Adjuvant and rMuPH20. Subsequent doses of rMuPH20 were administered via intramuscular injections with rMuPH20 mixed 1:1 with Incomplete Freund's Adjuvant. Whole blood samples from serial bleeds of the rabbits were processed to plasma using K2-EDTA and clarified by centrifugation at 1000g at 4°C for 10 min. Plasma was stored at 4°C prior to antibody purification.

The rMuPH20, which was tagged with a C-terminal FLAG octapeptide added for subsequent immunoaffinity purification (amino acid sequence DYKDDDDK), consisted of 481 amino acids: rMuPH20-K481-FLAG. The construct was cloned into lentiviral vector pLV-EF1a-MCS-IRES-GFP-Bsd (Biosettia, San Diego, CA). All vector construction, sequence verification, viral production, and viral titer determination were performed by Biosettia. The constructs were transduced into CHO-S cells cultured in CD-CHO media supplemented with 4 mmol/L

Glutamax (Invitrogen) and 4 μ g/mL Polybrene (Biosettia). Titered virus was added into each well using a multiplicity of infection of 10; infected cells were then incubated at 37°C for 6 h. Cells in replicate wells were harvested, pooled, and pelleted at low speed (1000 \times g). Approximately 4 days after initial infection, the media was supplemented with 2 μ g/mL of Blasticidin (Invitrogen). The media was changed every 3–4 days until CHO-S cells were approximately 90% confluent. The cells were then transferred to shaker flasks for antibody production.

Purification of anti-rMuPH20 antibodies

rMuPH20 reactive antibodies were purified from plasma by a sequential enrichment/exclusion process over a FLAG octapeptide affinity column (Sigma-Aldrich), followed by rMuPH20 affinity chromatography (Halozyme Therapeutics). Antibody concentrations were calculated using a Nanodrop 2000 UV-Vis spectrophotometer (Thermo-Scientific, Waltham, MA). Two to five liters of conditioned media were harvested and loaded on an anti-FLAG peptide immune-affinity column.

The ability of each antibody to detect its antigen was confirmed using western blot analysis with increasing amounts (25, 50, 100, and 200 ng) of the rMuPH20-FLAG protein (Halozyme Therapeutics). rMuPH20 was resolved by electrophoresis in a 4–20% SDS-PAGE gel under reducing conditions and transferred to polyvinylidene fluoride membrane. The blots were incubated overnight at 4°C with the two different rabbit polyclonal antibodies, Ab1637 or Ab2678, and then incubated with a goat anti-rabbit antibody conjugated with HRP for 1 h at ambient temperature, followed by incubation with tetramethylbenzidine. Staining was detected by imaging the blots using a Bio-Rad Chemi-Doc MP imaging system (Bio-Rad Life Sciences).

Characterization of the specificity of Ab1637 and Ab2678 anti-rMuPH20 antibodies

The specificity of the antibodies was evaluated by immunohistochemical staining of testis, brain, and spinal cord tissue sections of *Spam1* wild type (WT) and nullizygous mice²⁶ and *Hyal5* (a homologous sperm hyaluronidase) WT and nullizygous mice.^{27,28}

Results

Expression of *Spam1* mRNA was not detected in cultured murine OPCs

RT-qPCR analysis of *Spam1* expression was performed using RNA isolated from primary murine OPCs and from cultures of primary murine astrocytes and cortical

neurons, serving as positive controls for glial and neuronal cell markers. As a positive control for *Spam1* mRNA expression, mRNA was isolated from testis of adult male C57BL/6 mice (Table 4). As expected, in testis, steady-state expression of *Spam1* mRNA was prevalent with a cycle threshold (C(t)) value of 22, which correlated to 4.4×10^4 copies per 50 ng of input RNA. In contrast, no signal for *Spam1* mRNA was detected in any of the primary cell samples, including the enriched OPC sample after 45 cycles. Expression of β -actin was consistently abundant in all samples with C(t) values ranging between 16.6 and 18.5. In addition, expression was demonstrated for the OPC marker *PDGFR α* (C(t) values ranging from 22.3 to 27.4), and neuronal markers *Dcx* and *NeuN* (C(t) values ranging from 21.9 to 32.3 and 24.2 to 28.7, respectively). Elevated *PDGFR α* expression in primary OLs and *Dcx* and *NeuN* expression in neuronal cell cultures indicate that the cells were of the correct origin. These results demonstrate that *Spam1* mRNA transcripts were not detected in normal murine cells of neuronal origin.

OPC differentiation is inhibited by BTH IV-S but not rHuPH20

We were able to replicate the previously reported observations that BTH IV-S at 40 μ g/mL inhibited OPC myelination as detected by an anti-MBP antibody and that heat inactivation of BTH IV-S eliminated its inhibitory effect,¹⁶ demonstrating that a labile component of the BTH IV-S was likely responsible for the inhibition of OPC differentiation (Fig. 1A–C). In contrast, addition of 40 μ g/mL of highly purified rHuPH20 did not inhibit OPC differentiation (Fig. 1D). Quantification of the effect of the treatments on OPC differentiation is graphically presented as MBP-positive cells (three wells per treatment) as a percent of control (OPCDM) in Figure 1E. BTH IV-S had a significant inhibitory effect ($P < 0.05$, one-way ANOVA) compared with control and other treatments. No significant differences were observed between control, heat-inactivated BTH IV-S, or rHuPH20. These data suggest that the PH20 hyaluronidase enzymatic activity present in BTH IV-S was not responsible for the inhibition of OPC differentiation. Experiments in rat OPC culture provide additional evidence that neither PH20 nor PH20 digestion fragments inhibited OPC differentiation (Fig. S7).

BTH preparations contain multiple protein contaminants

SDS-PAGE and Coomassie staining of equivalent total protein loads (12 μ g) revealed that commercially available BTH IV-S and BTH VI-S (Sigma) are complex mixtures

of multiple proteins (Fig. 2), ranging in molecular weights; BTH IV-S appeared to contain more proteins at lower molecular weight range than BTH VI-S, while rHuPH20 showed a single band between 50 and 75 kDa.

To identify significant contaminating proteins, BTH IV-S was screened using a multiplex immunoassay against a panel of 59 analytes that included multiple cytokines, chemokines, and growth factors using RodentMAP v3.0 (Myriad RBM). Nine proteins were identified at levels greater than the lower limit of quantitation (LLOQ) (Table 5). bFGF concentrations were estimated to be >1150 ng/mL suggesting that the BTH IV-S sample contained significant amounts of bovine bFGF.

Quantitation of the bFGF levels in sigma BTH

The levels of bFGF in several samples of BTH IV-S, BTH VI-S, and rHuPH20 were determined using an ELISA (Table 6). Two different lots of Sigma BTH IV-S contained levels of bFGF (79–119 ng/mg). BTH VI-S contained considerably lower levels of bFGF (0.65–0.98 ng/mg). Highly purified rHuPH20 contained no detectable bFGF (<0.04 ng/mg).

bFGF at concentrations similar to that in BTH IV-S inhibits OPC differentiation

Sigma BTH IV-S used in culture at 100 U/mL (40 μ g/mL) would result in an estimated bFGF concentration between 3.2 and 9.4 ng/mL in the culture media. Therefore, the effects of bFGF at 5 and 10 ng/mL on OPC differentiation were tested using purified bovine bFGF (R&D Systems). The effects of 10 ng/mL bFGF relative to 40 μ g/mL of BTH IV-S and 40 μ g/mL rHuPH20 on untreated OPCs in OPCDM (control) are presented in Figure 3. bFGF and BTH IV-S, but not rHuPH20, significantly inhibited OPC myelination compared to untreated OPCs in OPCDM medium. These data demonstrate that bFGF at levels similar to those detected in BTH IV-S can inhibit OPC differentiation in vitro.

Reduction/Depletion or inhibition of bFGF in BTH IV-S eliminates inhibitory effects on OPC differentiation

The level of bFGF in BTH IV-S was reduced by immunodepletion to >90% of its original content using a neutralizing anti-FGF2 (bFGF) antibody and affinity chromatography (Fig. 4). The majority of bFGF was removed from BTH IV-S as shown in the flow-through fraction (Fig. 4, lane 2). Figure 4 (lane 3) shows the eluted fraction from Protein A/G Plus resin.

Table 4. Expression of Murine *Spam1* and Neuronal Markers in Cultured Oligodendrocyte Precursor Cells, Astrocytes, and Neurons.

	<i>Spam1</i>		<i>β-actin</i>		C(t)		
	C(t)	Copy Number/50 ng RNA	C(t)	Copy Number/50 ng RNA	<i>Dcx</i> ²	<i>PDGFRα</i> ³	<i>NeuN</i> ⁴
Primary Oligodendrocyte Precursors	>45	ND ¹	18.5	1.4 × 10 ⁷	24.2	22.3	29.4
Primary Astrocytes	>45	ND ¹	17.2	3.3 × 10 ⁶	29.3	27.0	28.7
Primary Cortical Neurons	>45	ND ¹	16.6	3.3 × 10 ⁶	21.9	27.4	24.2
Adult C57BL/6 Mouse Testis	22.0	4.4 × 10 ⁴	17.7	2.4 × 10 ⁶	32.3	25.9	29.2

C(t): Cycle threshold (45 total PCR cycles were run); *Spam1*-primer probe set specific for *Spam1*/PH20 gene; *β-actin*-primer probe set specific for housekeeping gene. Copy number was calculated as described in methods.

¹ND: not detected: 50 or 100 copies as a threshold.

²Doublecortin (*Dcx*): marker of developing neurons.

³Platelet-derived growth factor receptor (*PDGFRα*): marker of oligodendrocyte precursor cells.

⁴Neuronal nuclei (*NeuN*): neuron-specific marker.

Immunodepletion of bFGF from BTH IV-S eliminated its inhibitory effects on OPC differentiation (Fig. 5A). Further, treatment of OPCs with bFGF or BTH IV-S combined with 10 nmol/L of the pan-FGF receptor inhibitor PD173074 (inhibitor-Inh)²⁹ also eliminated the inhibitory effect on OPC differentiation (Fig. 5B). Incubation with PD173074 alone had no effect on OPC differentiation. BTH VI-S, bFGF, and rHuPH20 were included for comparison (Fig. 5A and B).

Oligodendrocytes produce HA which is digested by BTH IV-S and rHuPH20

To demonstrate the relevance of the system to detect PH20 hyaluronidase-dependent effects on OPC differentiation, the production of HA by differentiated OLs (OPCDM control) or after treatments with bFGF, BTH IV-S, or rHuPH20 was characterized by staining with bHABP and immunofluorescence (Fig. 6A–D). Additionally, the concentration of HA in the culture medium supernatant for each treatment was determined using an aggrecan binding assay (Fig. 6E). Differentiated OLs (OPCDM control) produced measurable amounts of cell-associated HA (Fig. 6A) and secreted soluble HA in the culture supernatant (155 ng/mL) (Fig. 6E, row 1). Treatment of OLs with 10 ng/mL bFGF did not reduce cell-associated HA labeling (Fig. 6B) or HA in the culture supernatant (219 ng/mL; Fig. 6E, row 2); whereas, the addition of 40 μg/mL of BTH IV-S reduced HA labeling of OLs (Fig. 6C) and HA in the culture supernatant to 4 ng/mL, which is below the LLOQ for the assay (Fig. 6E, row 3). Likewise, treatment of OLs with 40 μg/mL rHuPH20 also reduced cell-associated HA levels (Fig. 6D) and HA in the culture supernatant was 4 ng/mL (Fig. 6E, row 4).

Immunofluorescence detection of PH20 protein in CNS tissue

Detection of PH20 in the spinal cord and brain of control and EAE mice was evaluated by immunofluorescence labeling using two rabbit polyclonal antibodies directed against rMuPH20 (Halozyme Therapeutics), and shown by western blot to specifically detect a single band for rMuPH20. The tissue sections were colabeled with an anti-MBP antibody and DAPI. Mouse testis was used as a positive control tissue for PH20 expression. Characterization of the anti-rMuPH20 antibodies is shown in Figures S1–S6.

No specific labeling by Ab2678 or Ab1637 was observed in spinal cords of either control (Fig. 7A and D) or EAE spinal cord (Fig. 7B and E). As expected, both antibodies specifically labeled the germinal cells of the seminiferous tubules of mouse testis (Fig. 7C and F). Neither antibody labeled any aspect of corpus callosum, including the dense tracks of myelinated axons in the dentate gyrus (Fig. 8A and D) of either normal or EAE mice (Fig. 8B and E), but specifically labeled the germinal cells of the seminiferous tubules of mouse testis (Fig. 8C and F). These results strongly suggest that murine PH20 is not present in healthy or diseased mouse CNS tissues.

Characterization of HA and myelin staining in the spinal cord

The EAE mouse model is characterized by inflammatory processes affecting diverse parts of the CNS including the optic nerve,^{30,31} and the most obvious demyelinating lesions are observed in the spinal cord.^{19,20} In the transverse sections from the spinal cords of normal and EAE mice, staining for HA content demonstrated two distinct labeling patterns. In control mice, HA labeling was homogeneously

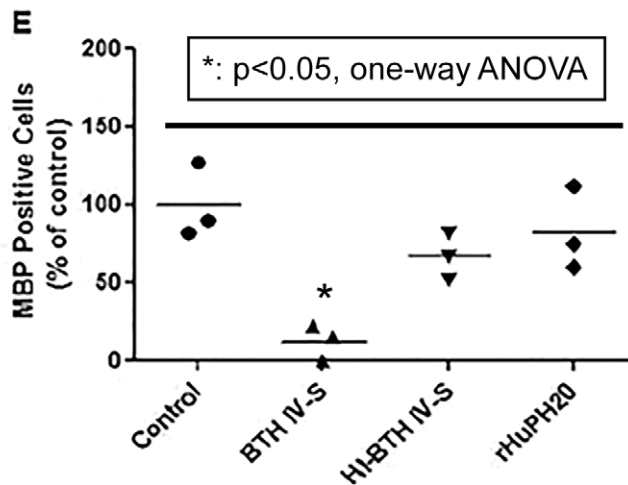
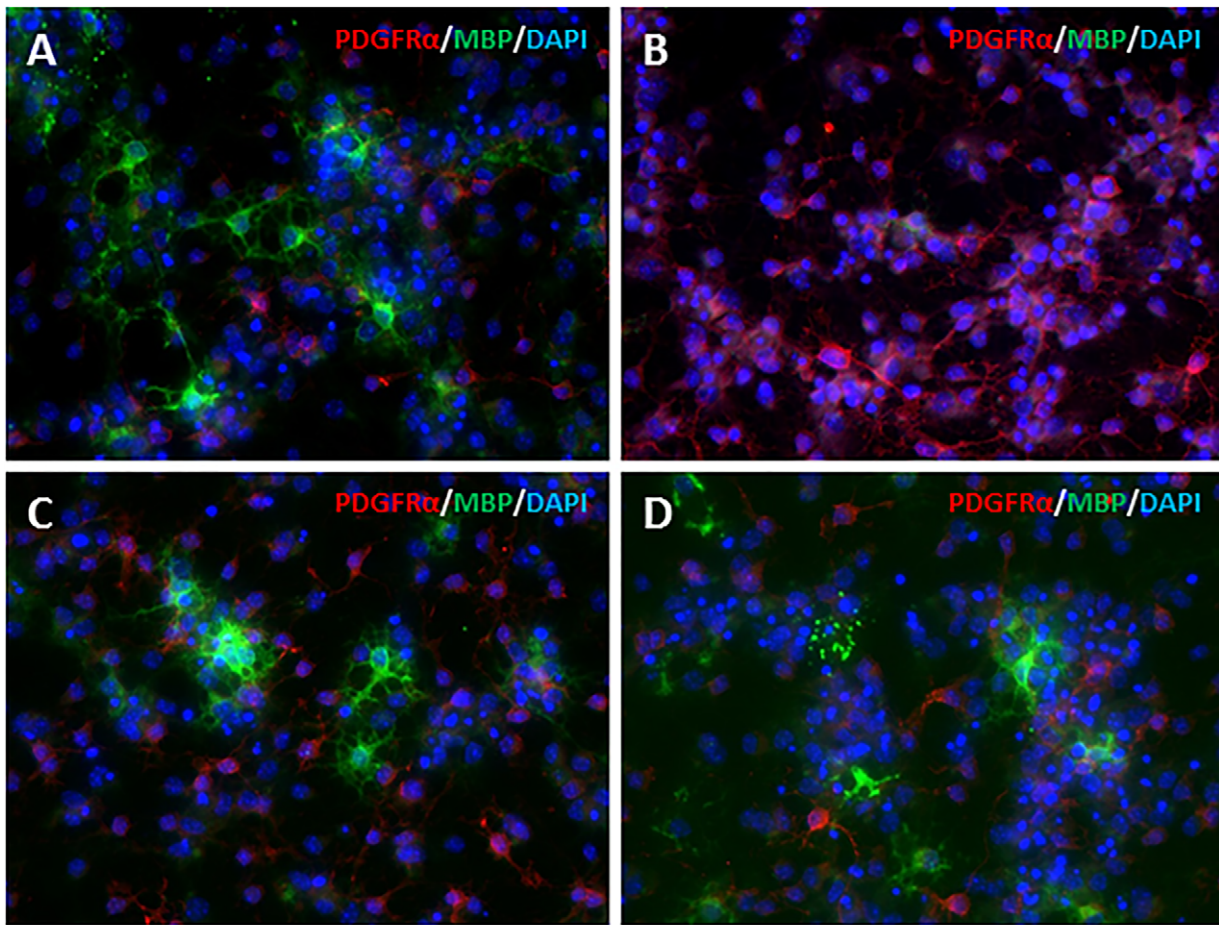


Figure 1. Inhibition of OPC myelination by bovine testicular hyaluronidase (BTH) is not correlated with PH20 enzymatic activity. (A) Mature OLs produced by culturing of OPCs in OPCDM without further treatment; (B) OLs cultured in OPCDM with 40 $\mu\text{g}/\text{mL}$ of BTH IV-S; (C) OLs cultured in OPCDM with 40 $\mu\text{g}/\text{mL}$ heat-inactivated BTH IV-S (HI-BTH IV-S); (D) OLs cultured in OPCDM with 40 $\mu\text{g}/\text{mL}$ rHuPH20. After incubation for 48–96 h, cultures were fixed and labeled for the OL lineage markers: *PDGFR α* (red, marker of OPCs), MBP (green, mature OLs), and DAPI (blue; cell nuclei). (All images: 20 \times objective magnification with optical zoom.) (E) Quantitation of maturation state of cells by counting MBP-positive cells (% of control, in OPCDM, panel A) following specified treatments. BTH IV-S, but not HI-BTH IV-S or rHuPH20 is significantly different from control (*: $P < 0.05$, one-way ANOVA).

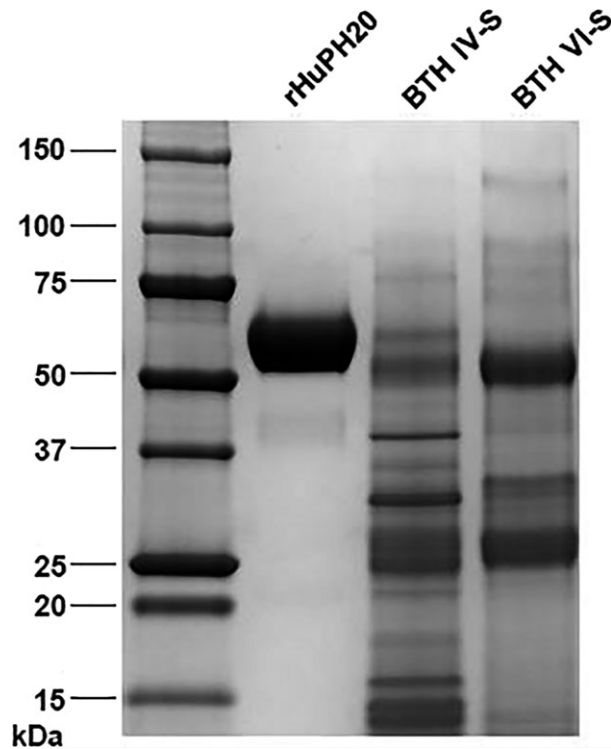


Figure 2. SDS-PAGE of rHuPH20, Sigma bovine testicular hyaluronidase (BTH) IV-S, and BTH VI-S hyaluronidase preparations. Proteins (12 μ g of total protein per sample) were resolved by SDS-PAGE and stained with Coomassie Blue. BTH IV-S and BTH VI-S preparations show multiple protein species with a wide range of molecular weights; rHuPH20 shows a single band of about 61 kDa.

distributed throughout the tissue sections (Fig. 9A). In the EAE mouse, HA content was greatly decreased in the demyelinating lesions of the spinal cord, whereas the regions more peripheral to the damaged areas showed discrete elevations in HA staining intensity (Fig. 9D). Tissue demyelination was complete in EAE spinal cord lesions and was accompanied by axonal degeneration (Fig. 9E).

Deep RNA sequencing of lumbar spinal cord and corpus callosum tissues

Total RNA from lumbar spinal cord and brain enriched for corpus callosum from normal (control) and EAE mice

Table 6. Quantikine ELISA evaluation of bFGF content of commercial hyaluronidase reagents.

Hyaluronidase (source/lot number)	bFGF concentration (ng/mg)
Hyal type IV-S (Sigma/SLBD1402V)	14–22
Hyal type IV-S (Sigma/SLBC1033V)	79–119
Hyal type VI-S (Sigma/117K7010V)	0.65–0.98
rHuPH20 (Halozyme/462-019B)	<0.04

bFGF, basic fibroblast growth factor; ELISA, enzyme-linked immunosorbent assay; Hyal, hyaluronidase; rHuPH20, recombinant human PH20.

was used for deep RNA sequencing analyses. Evaluations of changes in expression of selected genes known to be involved in HA synthesis (i.e., corresponding to the murine hyaluronan synthases 1, 2, or 3 which synthesize HA at the inner surface of the plasma membrane), metabolism (i.e., corresponding to the hyaluronidase gene/protein family that includes Hyals 1-5 and Spam1/PH20 which enzymatically degrade their substrate hyaluronan; and CD44, a well-established cellular receptor for hyaluronan), as well as housekeeping genes (i.e., Glyceraldehyde 3-phosphate dehydrogenase [GAPDH], RNA Polymerase II subunit A [Polr2a], Actin [actb] that all consistently used as markers for RNA quality and integrity) are presented in Figure 10. The fold change in mRNA expression in EAE versus control mouse spinal cord or corpus callosum is expressed as Log₂ (Fold Change EAE:Control) and presented in Figures 10A and B. In the EAE spinal cord, HA synthase 3 (*Has3*) expression was induced more than twofold compared to control, and hyaluronidases, *Hyal2* and *Hyal3*, were also elevated to a lesser extent. However, *Spam1*, *Hyal1*, and *Hyal5* mRNAs were not detected in either control or EAE spinal cord tissue. *Hyal4*, *Has2*, and *CD44* gene expression were detected and all were down-regulated in the EAE spinal cord compared to control mouse tissue. In the corpus callosum of the EAE mice, *Has2* and *CD44* as well as *Hyal1*, *Hyal3*, and *Has3* were all slightly increased compared to control mouse corpus callosum. However, there was no expression of *Spam1*, *Hyal2*, *Hyal4*, or *Hyal5*. HA synthase, *Has1* was present at low levels in controls and appeared to be down-regulated in EAE mice.

Table 5. Screening of proteins in Sigma BTH IV-S by RodentMAP analysis.

Analyte	Factor VII	FGF-9	bFGF	GH	Leptin	Lymphotoxin	MIP-1b	PAI-1	Resistin
RBM LLOQ (ng/mL)	3.8	0.57	3.1	0.31	0.011	4.3	11	0.0068	0.0077
BTH IV-S (ng/mL)	6.1	0.95	>1150	1.0	0.03	7.0	23	0.01	0.01

bFGF, basic fibroblast growth factor; BTH, bovine testicular hyaluronidase; FGF, fibroblast growth factor; GH, growth hormone; LLOQ, lower limit of quantitation; MIP, macrophage inflammatory protein; PAI, plasminogen activator inhibitor; RBM, RNA-binding motif antibody.

Overall, these data indicate that HA synthase and metabolic genes are expressed and regulated in the EAE inflammatory model of demyelination, but there is no expression of *Spam1* in the CNS of normal or EAE mice.

Directed query of the stanford proteome database for PH20 expression in the brain of normal adult and acute MS lesions

A directed query of the Stanford Proteome database revealed that PH20 protein was not detected in human MS brain lesions or control brain tissues. The entire database is available as described by Han and colleagues in their Supplementary Data.²⁴ In contrast, there was expression of the housekeeping protein β -actin; proteins associated with hyaluronan extracellular matrix, such as *CD44*, brevican, versican, and proteoglycan link protein 2; proteins and several other proteins proposed to be associated with MS disease pathogenesis, including low to moderate levels of Nogo. In addition, proteins associated with neuronal precursor cells and/or oligodendrocyte progenitor cells, including doublecortin and nestin were also detected.

Discussion

Hyaluronan is present in normal CNS tissue, and changes in HA synthesis and metabolism may provide important clues to understand disease processes and remodeling in inflammatory demyelinating conditions, including MS. In

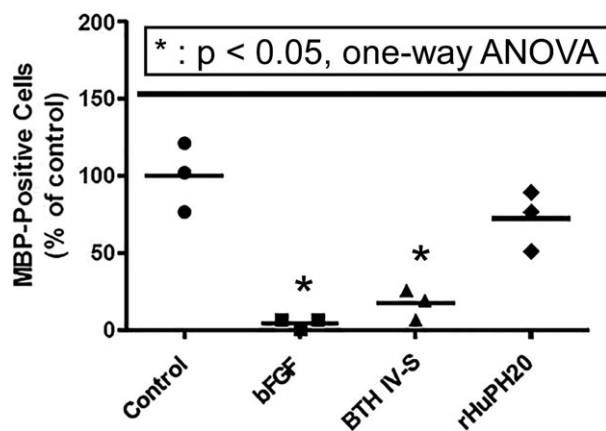


Figure 3. bFGF and bovine testicular hyaluronidase (BTH) IV-S similarly inhibit OPC differentiation. Evaluation of OPC differentiation cultured in OPCDM was performed on cells coincubated with 40 μ g/mL rHuPH20, 40 μ g/mL of BTH IV-S, or 10 ng/mL human recombinant bFGF. Only conditions where bFGF and BTH IV-S are added to the culture medium but not rHuPH20 displayed results significantly different from the control (*: $P < 0.05$, one-way ANOVA).

somatic tissues, regulation of HA levels is governed by a balance between HA synthases (*Has1*, *Has2*, *Has3*) and hyaluronidases (*Hyal1*, *Hyal2*, *Hyal3*, *Hyal4*); in contrast, PH20 and *Hyal5* (in the mouse) are reported to be primarily expressed in the adult male reproductive tract and play a nonessential role in fertilization.^{27,28}

Hyal2 has been reported to be expressed in brain during development, but Hyals in general appear to have low or no expression in healthy adult brain.³² However, following ischemic or traumatic brain injury, increased expression of non-PH20 Hyals (and HA degradation) have been reported in human and rat.^{33–35} Expression of *Hyal2* and *Hyal3* has also been reported in oligodendrocytes in vitro.^{16,36} *Hyal2* and *Hyal3* degrade hyaluronan and chondroitin sulfate,^{21,37} and HA turnover in the brain could be attributable to these enzymes, or potentially in part to a recently described protein, *KIAA1199*, which has been associated with hyaluronan depolymerizing activity.^{38,39} Alternative HA degradation pathways include cleavage by free oxygen radicals generated by inflammatory cells.^{40–42} Because HA may be important in

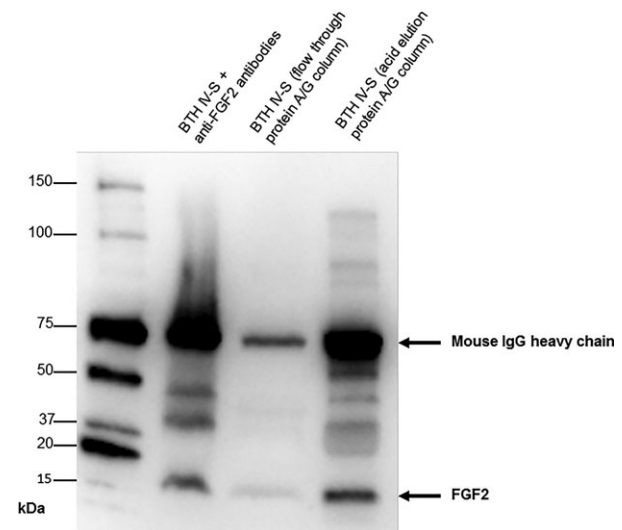


Figure 4. Western blot analysis of bFGF (FGF2)-depleted bovine testicular hyaluronidase (BTH) IV-S. bFGF depletion from BTH IV-S was carried out by immunoprecipitation using a neutralizing anti-FGF2 antibody (anti-FGF2, EMD Millipore) and subsequent removal by Protein A/G affinity chromatography. Samples were then analyzed by SDS-PAGE under reducing conditions followed by western blot analysis. The membrane was treated with a primary mouse anti-bFGF antibody (anti-FGF2, EMD Millipore) and a goat anti-mouse HRP as the secondary antibody (EMD Millipore). The Amersham ECL Advance Western Blotting Detection Kit (GE Healthcare) was used for signal development. Lane 1: Western blot protein marker (Bio-Rad Life Science). Lane 2: BTH IV-S mixed with neutralizing anti-FGF2 prior to passing through Protein A/G resin. Lane 3: Flow-through fraction from Protein A/G resin spin column. Lane 4: Eluted fraction from Protein A/G resin using 0.1 mol/L glycine, pH 2.5.

many neurological processes and diseases,⁴³ it is important to study the regulation of HA metabolic proteins including hyaluronidases and hyaluronan synthases. These recent reports support a role of HA and hyaluronidases in remodeling the extracellular matrix of the CNS during development and following injury. However, until recently published reports that *Spam1*/PH20 may also be expressed in normal CNS tissues and up-regulated in inflammatory demyelinating CNS of mouse, human, and fetal sheep,^{16,17,36} there have been no other reports of PH20 in the CNS.

To critically evaluate whether PH20 is expressed in CNS tissues, we used multiple orthogonal methods to explore expression of the *Spam1* gene and PH20 protein. Techniques used to detect PH20 expression included the use of custom-made antibodies, RNA-Seq technology as well as interrogation of pre-established proteomic and genomic databases. Results from our expression analyses using multiple sensitive techniques yielded results consistent with the broader literature where expression of multiple hyaluronidases and hyaluronan synthases is reported but no expression of PH20 is observed.

We were unable to detect *Spam1* mRNA in primary murine OPCs, astrocytes, or neurons by RT-qPCR using a murine *Spam1* primer probe set, but detected expression in the adult mouse testis. Although highly sensitive

RNA-Seq analysis did not demonstrate PH20 expression in CNS tissue, we also attempted to replicate the experiments reported by Preston et al.¹⁶ using the reported primers and less sensitive RT-PCR techniques. We were unable to detect any *Spam1* messenger RNA in CNS tissue, and only detected *Spam1* RNA in testis samples (positive control) when using low stringency PCR amplification conditions.

We demonstrated that rHuPH20 did not inhibit OPC differentiation in vitro, and identified bFGF, a significant contaminant of commercial BTHs, as the likely cause of BTH's inhibitory effects on OPC differentiation. Growth factors bFGF and PDGF α are known inducers of OPC proliferation and inhibitors of OPC maturation.^{44–46} bFGF is thought to inhibit late OPC differentiation into mature OLs by inducing withdrawal of myelin sheaths and down-regulating expression of the major myelin proteins including MBP.^{47,48}

Commercial BTHs have been shown to be a complex mixture of proteins and other nonprotein proinflammatory contaminants, and contain <1% PH20 hyaluronidase.^{21,49} However, reports on commercial BTH contaminations have continued to be largely ignored by the broader research community, when using BTHs as a source of PH20.^{21,50} Our investigations of contaminants in BTH are further supported by the recent report that

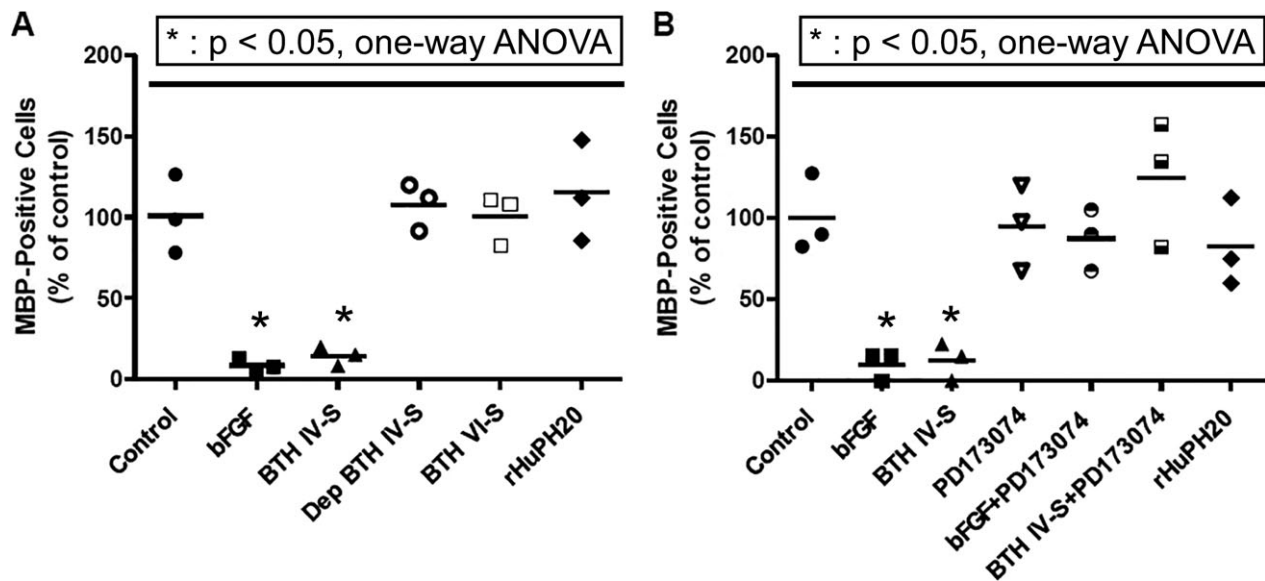
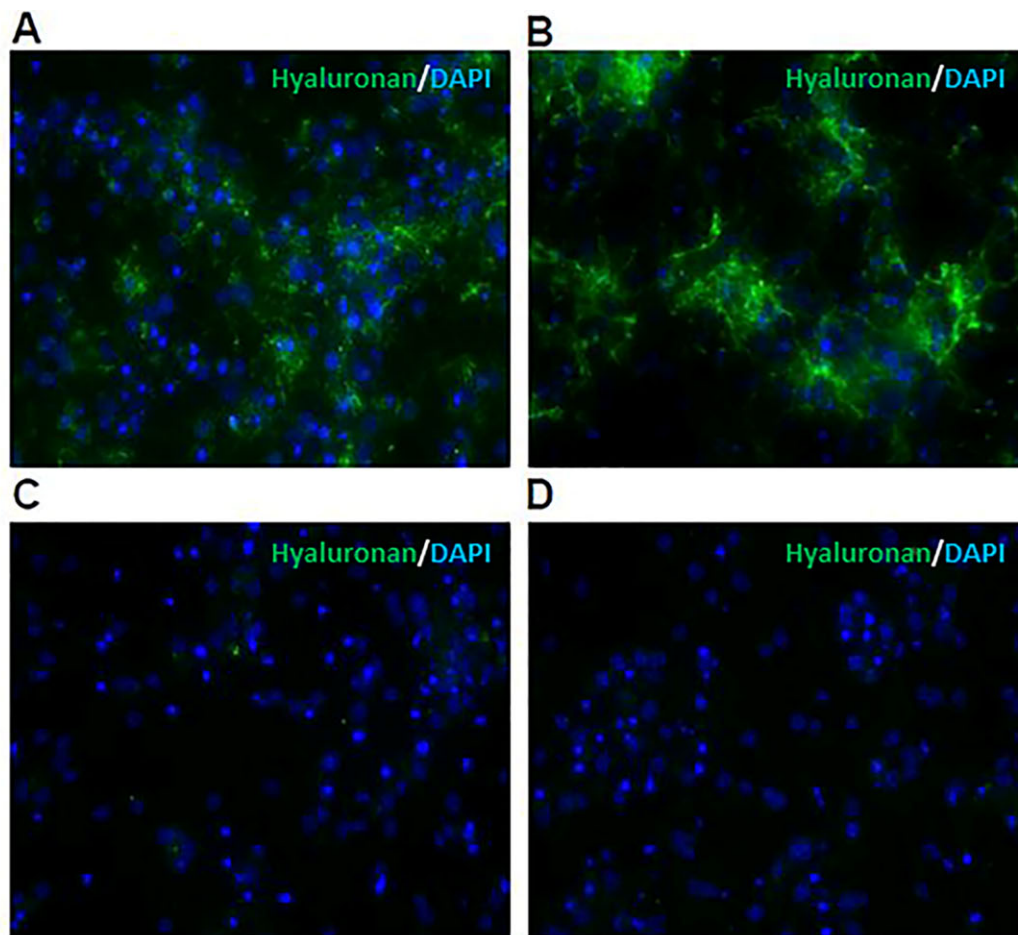


Figure 5. Depletion or pharmacological inhibition of bFGF in bovine testicular hyaluronidase (BTH) preparations eliminates BTH inhibitory effect on OPC differentiation. Quantitation of MBP cell analyses were conducted as described in Methods. (A) Depletion (Dep) of bFGF (>90%) from BTH VI-S significantly reduces the inhibitory effect of BTH IV-S as compared to control (*: $P < 0.05$, one-way ANOVA; ns: not significant). Further, highly purified rHuPH20 and another Sigma BTH (BTH VI-S) shown to contain significantly lower levels of bFGF (See Table 6) did not significantly inhibit OPC differentiation (*: $P < 0.05$, one-way ANOVA; ns: not significant); (B) treatment of cells with bFGF or BTH IV-S along with incubation with the small molecule bFGF receptor inhibitor PD173074 significantly reduces the inhibitory effect of both bFGF and BTH IV-S (*: $P < 0.05$, one-way ANOVA) on OPC differentiation.

injection of BTH IV-generated HA fragments, but not rHuPH20-generated or in vitro synthesized HA fragments (Select-HA 250K and HA 200K), resulted in inflammatory responses in a mouse air pouch model, as measured by stimulation of proinflammatory cytokine or chemokine production.⁵⁰ The literature reports of contaminants in both commercial BTHs and HA preparations suggest that

many of the reported effects attributed to PH20 and low molecular weight HA fragments may be due to contaminants, and indicate that caution is warranted when drawing conclusions about the biological activities of PH20 and PH20-specific HA digestion products when using commercial reagents. Further, since the HA fragments used in the lysolecithin model of demyelination



E

Culture condition	HA concentration, supernatant (ng/mL)
1. Control	155
2. bFGF (10ng/mL)	219
3. BTH IV-S (40μg/mL)	ND ^a
4. rHuPH20 (40μg/mL) pre-fixation	ND ^a

^a HA levels below the LLOQ for the ELISA assay (< 4ng/mL)

Figure 6. OLs produce HA which is digested by bovine testicular hyaluronidase (BTH) IV-S and rHuPH20. OPCs were grown in OPCDM to produce mature OLs with or without specified treatments. Cells were fixed and labeled with bHABP. Alexa Fluor 488-conjugated Streptavidin (green) was used to visualize HA. The cells were counterstained with DAPI (blue). (A) Cells in OPCDM without further treatment; (B) cells treated with 10 ng/mL bFGF; (C) cells treated with 40 μg/mL BTH IV-S; (D) cells treated with 40 μg/mL rHuPH20. (All images: 20 × objective magnification with optical zoom.) (E) Concentration of HA in supernatant measured by ELISA.

performed by Preston et al.¹⁶ were also generated using Sigma BTH IV-S, those results should be further investigated as well.

In expression studies of the spinal cord and brain tissues of normal and EAE mice, we were unable to confirm the presence of *Spam1* mRNA using deep RNA

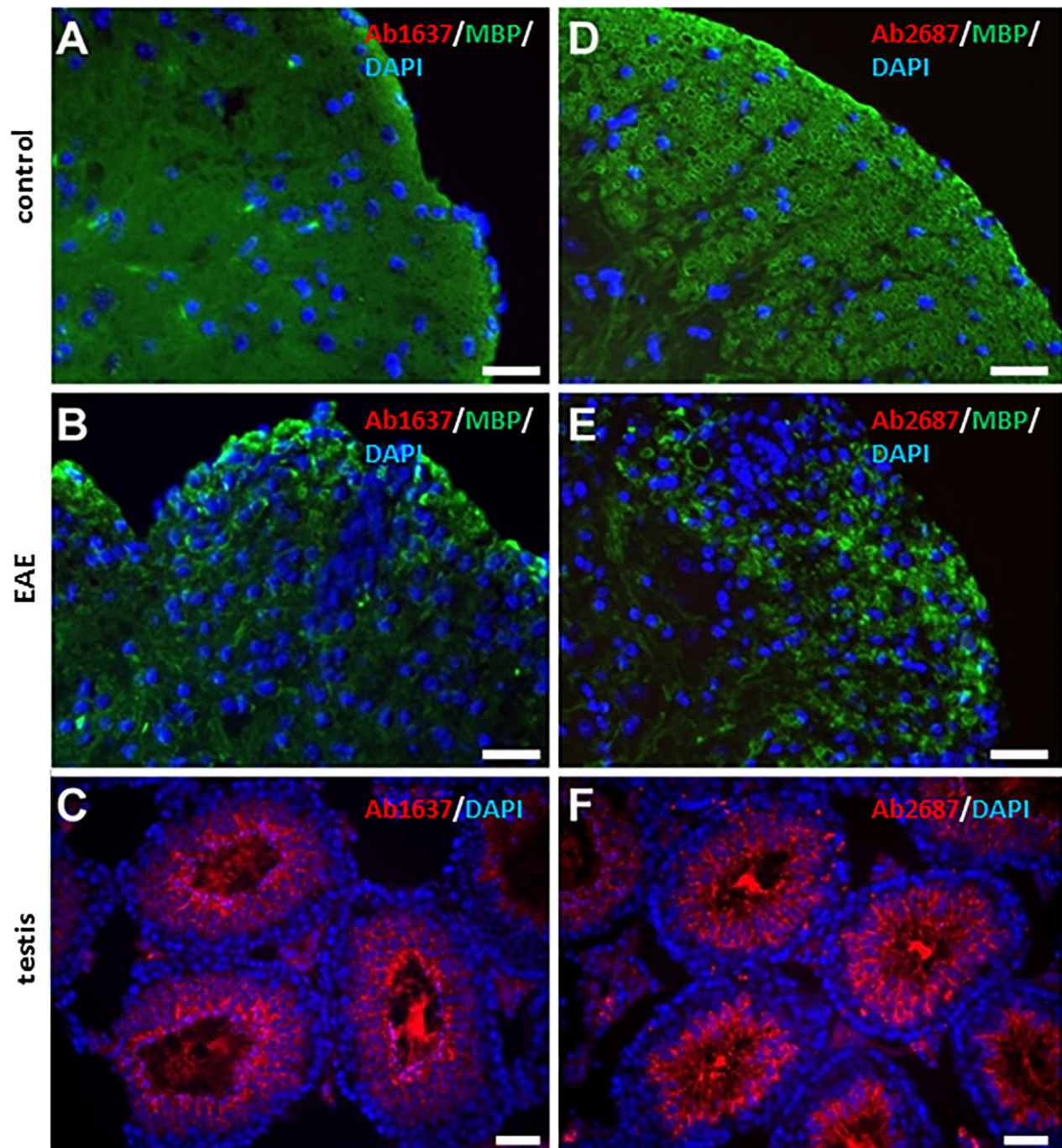


Figure 7. MuPH20 is not detected in the lumbar spinal cord of normal or experimental autoimmune encephalomyelitis (EAE) mice. Transverse sections of mouse spinal cord (A, B, D, E) were colabeled with a commercially available mouse anti-MBP antibody and the polyclonal rabbit anti-rMuPH20 antibodies Ab1637 (A, B) and Ab2687 (D, E) raised against rMuPH20. Tissue sections of mouse testis (C, F) were labeled with Ab1637 (C) and Ab2687 (F). Each representative photomicrograph was pseudocolored, anti-MBP labeling in green, anti-murine PH20 in red and the nuclei were stained with DAPI in blue. Scale bar = 50 μ m.

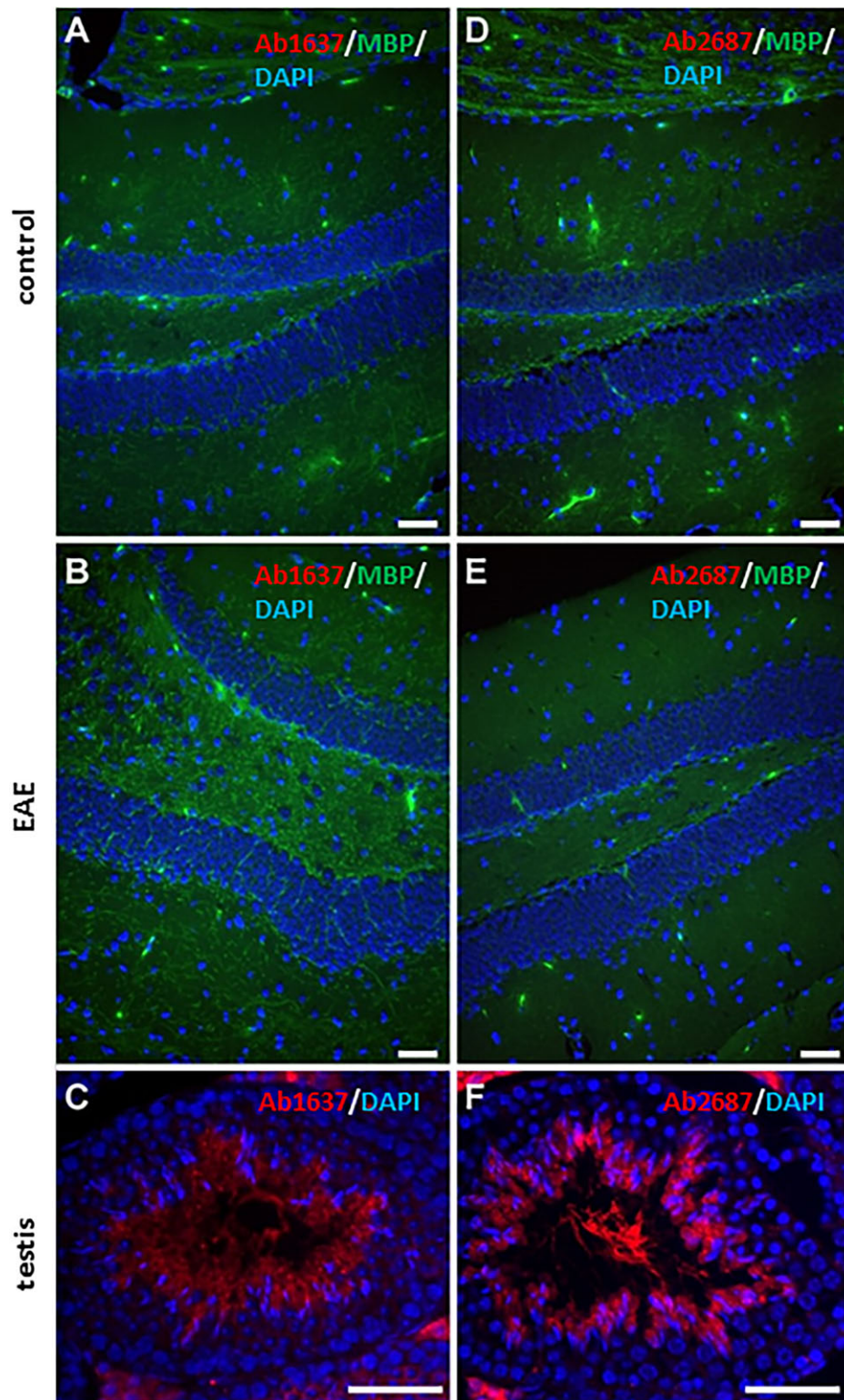


Figure 8. MuPH20 is not detected in the brain of normal or experimental autoimmune encephalomyelitis (EAE) mice. Coronal sections of mouse brain (A, B, D, E) were colabeled with a commercially available mouse anti-MBP antibody (Green) and the polyclonal rabbit anti-rMuPH20 antibodies Ab1637 (A, B) and Ab2687 (D, E) (Red) directed against murine PH20. Tissue sections of mouse testis (C, F) were labeled with Ab1637 (C) and Ab2687 (F). Scale bar = 50 μ m.

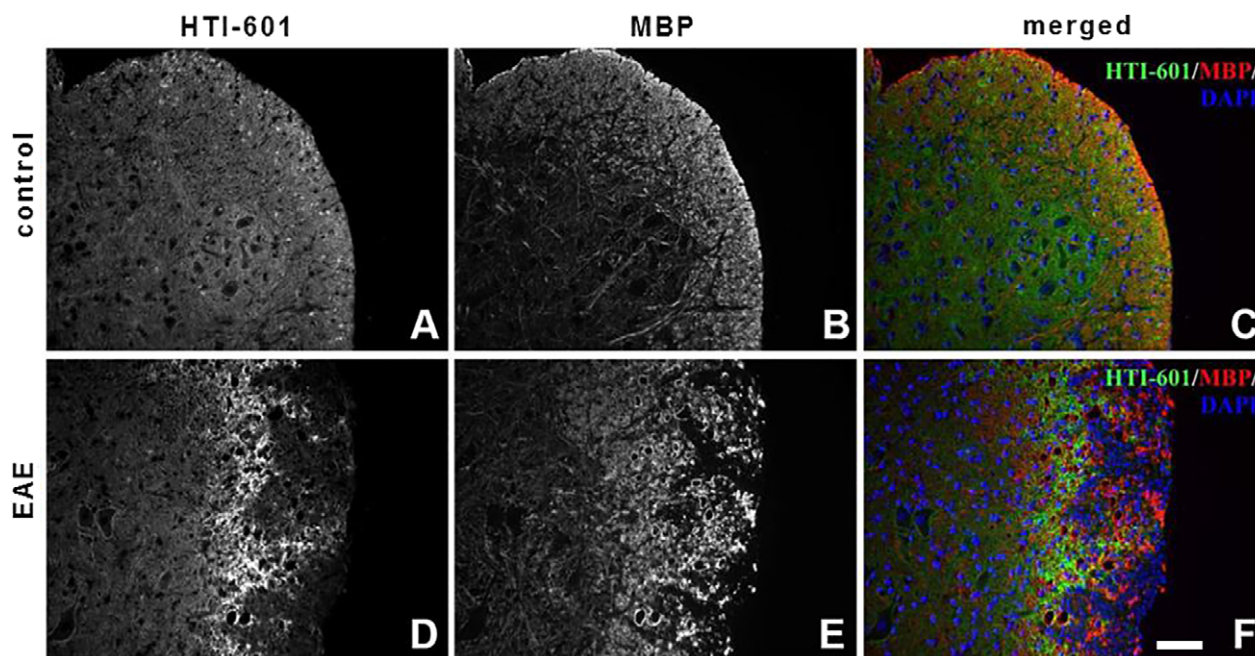


Figure 9. Characterization of HA and myelin staining in the normal and experimental autoimmune encephalomyelitis (EAE) spinal cord. Transverse sections of normal mouse spinal cord (A, B, C) or MOG EAE (D, E, F) were colabeled with the TSG-6- Δ Hep-Fc probe (HTI-601)²⁵ for histolocalization of hyaluronan (A, D) and a commercially available mouse anti-MBP antibody, MBP (B, E). Each representative photomicrograph was pseudocolored, HT-601 in green, anti-MBP labeling in red, and the nuclei were stained with DAPI in blue (C, F). Scale bar = 50 μ m.

sequencing methods. Further, we were unable to detect PH20 staining by immunohistological methods using two independent rabbit polyclonal antibodies directed against rMuPH20 that have been shown to selectively detect PH20 and the highly homologous Hyal5 protein (Fig. S1–S3).

Our inability to detect *Spam1*/PH20 expression in the CNS of normal adult or EAE mice is supported by our directed query of the Stanford MS Proteome database.²⁴ In our query, no PH20 protein expression was detected in brain lesions from human MS patients or age-matched control human brain tissue, though other HA metabolic and interacting proteins and housekeeping proteins were detected. Our expression data are also consistent with queries of other academic and public transcriptome and proteome databases, including CNS,^{51–55} which also confirm expression of HA metabolic and interacting proteins in the CNS, but not PH20, Hyal4, or Hyal5 (in the mouse).

Our characterization of histolocalization of HA in control and EAE mice confirmed that HA was homogeneously distributed throughout the spinal cord in normal animals, whereas in the EAE spinal cords, no HA was detected within the demyelinated areas, but was focally increased at the periphery of these damaged regions. The HA content in the brain was not significantly different

between control and EAE mice, though deep RNA sequencing expression data indicated that both HA synthases and Hyals were differentially up-regulated, suggesting some remodeling of HA in the EAE mouse brain.

The increase in HA levels adjacent to demyelinated regions of the spinal cord may result from increases in expression of hyaluronan synthase (*Has*) genes. RNA sequencing data demonstrated a two- to fourfold increase in steady-state *Has3* mRNA levels in the spinal cord and brain of EAE mice, and more variable changes in expression of *Has2*. *Has1* and *Has3* have also been reported to be expressed in developing spinal cord and *Has3* is the only isoform identified in the mature spinal cord.⁵⁶ Further, up-regulation of expression of HA synthases has been reported in inflammatory cells and neurons in perinfarcted regions following ischemic and traumatic injury,^{35,57–59} and in patients with Alzheimer's disease and age-related vascular brain injury.^{60–62} HA is also elevated in the brains of aged rodents and nonhuman primates.^{63,64}

A temporal relationship between HA synthases and accumulation of HA around damaged areas of the brain in response to neuronal damage are thought to stabilize the neuronal microenvironment.⁶⁵ However, HA accumulation around demyelinated lesions has also been proposed to prevent OPC maturation and remyelination.^{19,36}

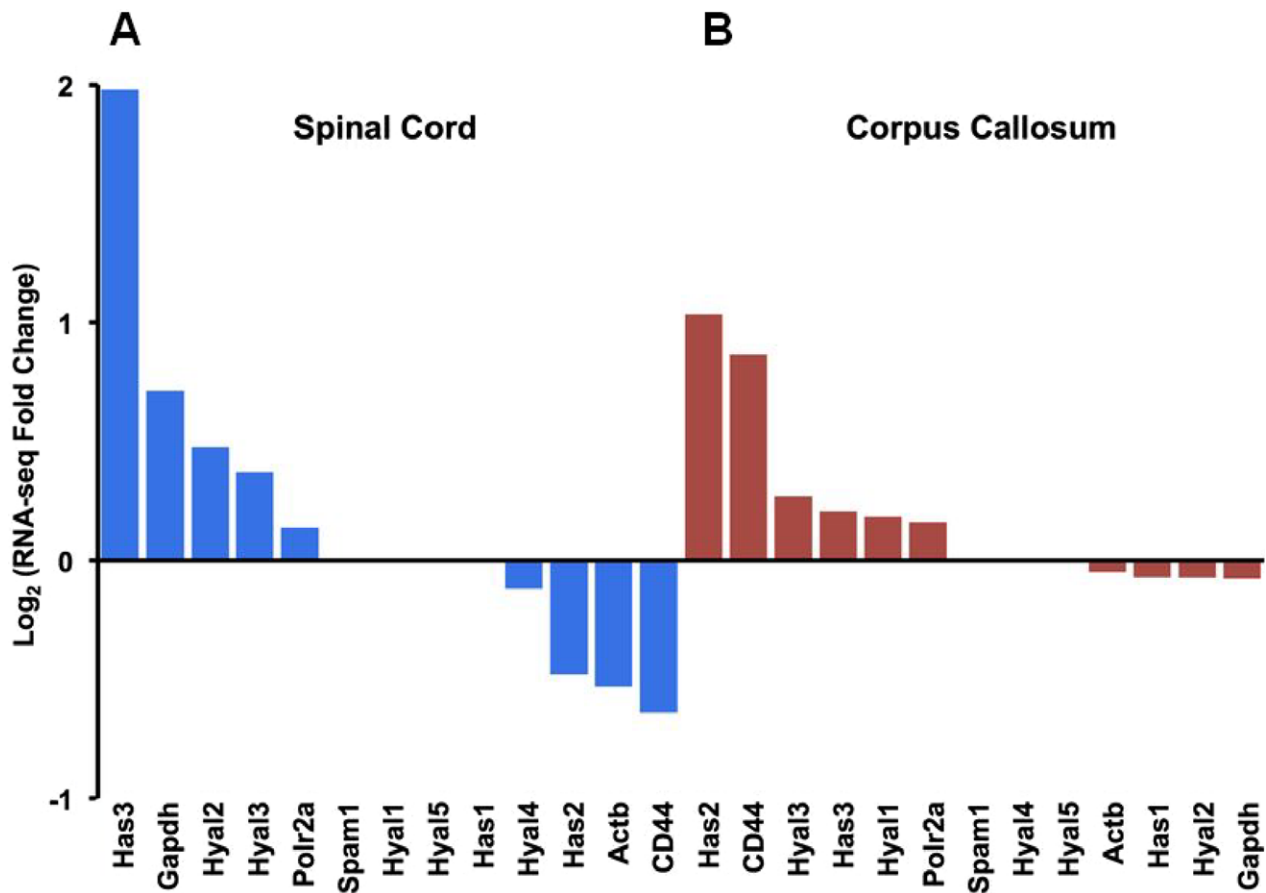


Figure 10. Summary of Deep RNA sequencing analysis of lumbar spinal cord and corpus callosum tissues of normal and experimental autoimmune encephalomyelitis (EAE) mouse. RNA sequencing (RNA-seq) data analyses of *Spam1* mRNA expression, other selected hyaluronan metabolic genes, and housekeeping genes are presented as Log₂ (RNA-Seq. fold change) between control and EAE tissues. Data are represented as a waterfall plot for spinal cord (A) and corpus callosum (B).

Thus, the relationship between HA polymer size and biological activity remains poorly understood.^{37,66} Recently, an important role has been ascribed to *Has3* since it has been shown that *Has3*-deficient mice have altered neuronal activity and seizures, which has been thought to result from reduction in brain extracellular space.⁶⁷

Our inability to replicate the key finding by Preston et al.¹⁶ of *Spam1*/PH20 expression in OPCs in culture or in the CNS of control and EAE mice, coupled with our finding that rHuPH20 or HA digestion products of PH20 did not inhibit OPC differentiation, casts doubt on the hypothesis that PH20-specific low molecular weight HA digestion products are responsible for the inhibition of OPC differentiation and remyelination. Other experimental results from this study support the earlier observations¹⁹ that HMW HA does inhibit OPC differentiation (Fig. S7). In addition, study of the biochemistry of the hyaluronidases has provided evidence that both bacterial and mammalian hyaluronidases create the same HA

degradation products.³⁷ These results, together with our finding that the inhibition of OPC differentiation by commercial BTHs is due in part to the presence of bFGF, suggest that the recent reports of *Spam1*/PH20 expression in the CNS may be reagent- and/or methods-specific and raises doubt about the proposed role of PH20 in the pathogenesis of neurodegenerative diseases. Other mechanisms of HA degradation and remodeling including the role of oxidative stress, other Hyals and HA synthases known to be expressed in the CNS, should be further investigated to better understand the role of HA in disease processes in the CNS.

Acknowledgments

The authors thank the technical and scientific staff members at Biomodels, LLC, including Ryan Dell and Jenny Tsui for assistance with data collection and animal care, and the remainder of the animal care staff members: Scott

Anderson, Samantha Rogers, Ingrid Rankin, Sean Graham, Martina Rosado, and Brett Van Dam; Rose Sekulovich from Halozyme Therapeutics, Inc., for handling the RNA sequencing contracts; and Lauryn D. Uribe for editing. The authors also acknowledge financial support from Baxter International.

Author Contributions

Paula J. Lapinskas: Design, oversight, and data analyses of *in vivo* studies. Mathieu Marella, Arnold B. Gelb: Design, implementation, and data analyses of IHC/IF studies and characterization of selectivity of the Anti-rMuPH20 antibodies. Joe Ouyang, Chunmei Zhao, Zhongdong Huang: Design, implementation, and data analyses of OPC studies and biochemical characterization of BTHs. Jonathan Zombeck: Ran the MOG EAE *in vivo* study, sample collection, and data analyses. Lei Huang, Robert Connor, Kim B. Phan: Produced the recombinant murine PH20 and Hyal5 proteins, production and purification of Anti-rMuPH20 antibodies, and specificity of proteins. Michael C. Jorge, Marie Printz, Rudolph D. Paladini, Barry Sugarman: Design, execution and data analysis of RT-qPCR studies. Ge Wei: Coauthor and generation of critical reagents. Gregory I. Frost, H. Michael Shepard, Daniel C. Maneval: Overall oversight of study designs and approval and financial support of studies. Barry Sugarman: Design and oversight of deep RNA sequencing, RNA sample preparation strategy, and data analyses. Lawrence Steinman: Scientific oversight and reviewed and performed the directed query of the Stanford Multiple Sclerosis Proteome Database.

Conflicts of Interest

All work was funded by Halozyme Therapeutics, Inc. All authors are employees or consultants for Halozyme Therapeutics, Inc., and declare no other conflict of interest.

References

- Jones MH, Davey PM, Aplin H, Affara NA. Expression analysis, genomic structure, and mapping to 7q31 of the human sperm adhesion molecule gene SPAM1. *Genomics* 1995;29:796–800.
- Csoka AB, Frost GI, Stern R. The six hyaluronidase-like genes in the human and mouse genomes. *Matrix Biol* 2001;20:499–508.
- Dunn CA, Mager DL. Transcription of the human and rodent SPAM1/PH-20 genes initiates within an ancient endogenous retrovirus. *BMC Genom* 2005;6:47.
- Lin Y, Mahan K, Lathrop WF, et al. A hyaluronidase activity of the sperm plasma membrane protein PH-20 enables sperm to penetrate the cumulus cell layer surrounding the egg. *J Cell Biol* 1994;125:1157–1163.
- Myles DG, Primakoff P. Why did the sperm cross the cumulus? To get to the oocyte. Functions of the sperm surface proteins PH-20 and fertilin in arriving at, and fusing with, the egg. *Biol Reprod* 1997;56:320–327.
- Martin-DeLeon PA. Germ-cell hyaluronidases: their roles in sperm function. *Int J Androl* 2011;34(5 Pt 2):e306–e318.
- Zhou C, Kang W, Baba T. Functional characterization of double-knockout mouse sperm lacking SPAM1 and ACR or SPAM1 and PRSS21 in fertilization. *J Reprod Dev* 2012;58:330–337.
- Deng X, He Y, Martin-DeLeon PA. Mouse Spam1 (PH-20): evidence for its expression in the epididymis and for a new category of spermatogenic-expressed genes. *J Androl* 2000;21:822–832.
- Evans EA, Zhang H, Martin-DeLeon PA. SPAM1 (PH-20) protein and mRNA expression in the epididymides of humans and macaques: utilizing laser microdissection/RT-PCR. *Reprod Biol Endocrinol* 2003;1:54.
- Kim E, Yamashita M, Kimura M, et al. Sperm penetration through cumulus mass and zona pellucida. *Int J Dev Biol* 2008;52:677–682.
- Zhang H, Martin-DeLeon PA. Mouse Spam1 (PH-20) is a multifunctional protein: evidence for its expression in the female reproductive tract. *Biol Reprod* 2003;69:446–454.
- Grigorieva A, Griffiths GS, Zhang H, et al. Expression of SPAM1 (PH-20) in the murine kidney is not accompanied by hyaluronidase activity: evidence for potential roles in fluid and water reabsorption. *Kidney Blood Press Res* 2007;30:145–155.
- Beech DJ, Madan AK, Deng N. Expression of PH-20 in normal and neoplastic breast tissue. *J Surg Res* 2002;103:203–207.
- El Hajjaji H, Cole AA, Manicourt DH. Chondrocytes, synoviocytes and dermal fibroblasts all express PH-20, a hyaluronidase active at neutral pH. *Arthritis Res Ther* 2005;7:R756–R768.
- Godin DA, Fitzpatrick PC, Scandurro AB, et al. PH20: a novel tumor marker for laryngeal cancer. *Arch Otolaryngol Head Neck Surg* 2000;126:402–404.
- Preston M, Gong X, Su W, et al. Digestion products of the PH20 hyaluronidase inhibit remyelination. *Ann Neurol* 2013;73:266–280.
- Hagen MW, Riddle A, McClendon E, et al. Role of recurrent hypoxia-ischemia in preterm white matter injury severity. *PLoS ONE* 2014;9:e112800.
- Wanisch K, Kovac S, Schorge S. Tackling obstacles for gene therapy targeting neurons: disrupting perineural nets with hyaluronidase improves transduction. *PLoS ONE* 2013;8:e53269.
- Back SA, Tuohy TM, Chen H, et al. Hyaluronan accumulates in demyelinated lesions and inhibits

- oligodendrocyte progenitor maturation. *Nat Med* 2005;11:966–972.
20. Basso AS, Frenkel D, Quintana FJ, et al. Reversal of axonal loss and disability in a mouse model of progressive multiple sclerosis. *J Clin Invest*. 2008;118:1532–1543.
 21. Bookbinder LH, Hofer A, Haller MF, et al. A recombinant human enzyme for enhanced interstitial transport of therapeutics. *J Control Release* 2006;114:230–241.
 22. Fang S, Hays Putnam AM, LaBarre MJ. Kinetic investigation of recombinant human hyaluronidase PH20 on hyaluronic acid. *Anal Biochem* 2015;480:74–81.
 23. Robinson WH, Utz PJ, Steinman L. Genomic and proteomic analysis of multiple sclerosis Opinion. *Curr Opin Immunol* 2003;15:660–667.
 24. Han MH, Hwang SI, Roy DB, et al. Proteomic analysis of active multiple sclerosis lesions reveals therapeutic targets. *Nature* 2008;451:1076–1081.
 25. Jadin L, Huang L, Wei G, et al. Characterization of a novel recombinant hyaluronan binding protein for tissue hyaluronan detection. *J Histochem Cytochem* 2014;62:672–683.
 26. Baba D, Kashiwabara S, Honda A, et al. Mouse sperm lacking cell surface hyaluronidase PH-20 can pass through the layer of cumulus cells and fertilize the egg. *J Biol Chem* 2002;277:30310–30314.
 27. Kim E, Baba D, Kimura M, et al. Identification of a hyaluronidase, Hyal5, involved in penetration of mouse sperm through cumulus mass. *Proc Natl Acad Sci USA* 2005;102:18028–18033.
 28. Kimura M, Kim E, Kang W, et al. Functional roles of mouse sperm hyaluronidases, HYAL5 and SPAM1, in fertilization. *Biol Reprod* 2009;81:939–947.
 29. Bansal R, Magee S, Winkler S. Specific inhibitor of FGF receptor signaling: FGF-2-mediated effects on proliferation, differentiation, and MAPK activation are inhibited by PD173074 in oligodendrocyte-lineage cells. *J Neurosci Res* 2003;74:486–493.
 30. Knier B, Rothhammer V, Heink S, et al. Neutralizing IL-17 protects the optic nerve from autoimmune pathology and prevents retinal nerve fiber layer atrophy during experimental autoimmune encephalomyelitis. *J Autoimmun* 2015;56:34–44.
 31. Rothhammer V, Heink S, Petermann F, et al. Th17 lymphocytes traffic to the central nervous system independently of alpha4 integrin expression during EAE. *J Exp Med* 2011;208:2465–2476.
 32. Triggs-Raine B, Salo TJ, Zhang H, et al. Mutations in HYAL1, a member of a tandemly distributed multigene family encoding disparate hyaluronidase activities, cause a newly described lysosomal disorder, mucopolysaccharidosis IX. *Proc Natl Acad Sci USA* 1999;96:6296–6300.
 33. Al'Qteishat A, Gaffney J, Krupinski J, et al. Changes in hyaluronan production and metabolism following ischaemic stroke in man. *Brain* 2006;129(Pt 8):2158–2176.
 34. Al Qteishat A, Gaffney JJ, Krupinski J, Slevin M. Hyaluronan expression following middle cerebral artery occlusion in the rat. *NeuroReport* 2006;17:1111–1114.
 35. Xing G, Ren M, Verma A. Divergent temporal expression of hyaluronan metabolizing enzymes and receptors with craniotomy vs. controlled-cortical impact injury in rat brain: a pilot study. *Front Neurol* 2014;5:173.
 36. Sloane JA, Batt C, Ma Y, et al. Hyaluronan blocks oligodendrocyte progenitor maturation and remyelination through TLR2. *Proc Natl Acad Sci USA* 2010;107:11555–11560.
 37. Stern R, Jedrzejewski MJ. Hyaluronidases: their genomics, structures, and mechanisms of action. *Chem Rev* 2006;106:818–839.
 38. Yoshida H, Nagaoka A, Kusaka-Kikushima A, et al. KIAA1199, a deafness gene of unknown function, is a new hyaluronan binding protein involved in hyaluronan depolymerization. *Proc Natl Acad Sci USA* 2013;110:5612–5617.
 39. Nagaoka A, Yoshida H, Nakamura S, et al. Regulation of hyaluronan (HA) metabolism mediated by HYBID (HYaluronan binding protein involved in HA depolymerization, KIAA1199) and HA synthases in growth factor-stimulated fibroblasts. *J Biol Chem* 2015;290:30910–30923.
 40. Myint P, Deeb DJ, Beaumont PC, et al. The reactivity of various free radicals with hyaluronic acid: steady-state and pulse radiolysis studies. *Biochim Biophys Acta* 1987;925:194–202.
 41. Uchiyama H, Dobashi Y, Ohkouchi K, Nagasawa K. Chemical change involved in the oxidative reductive depolymerization of hyaluronic acid. *J Biol Chem* 1990;265:7753–7759.
 42. Moseley R, Waddington RJ, Embury G. Degradation of glycosaminoglycans by reactive oxygen species derived from stimulated polymorphonuclear leukocytes. *Biochim Biophys Acta* 1997;1362:221–231.
 43. Senkov O, Andjus P, Radenovic L, et al. Neural ECM molecules in synaptic plasticity, learning, and memory. *Prog Brain Res* 2014;214:53–80.
 44. McKinnon RD, Smith C, Behar T, et al. Distinct effects of bFGF and PDGF on oligodendrocyte progenitor cells. *Glia* 1993;7:245–254.
 45. Baron W, Metz B, Bansal R, et al. PDGF and FGF-2 signaling in oligodendrocyte progenitor cells: regulation of proliferation and differentiation by multiple intracellular signaling pathways. *Mol Cell Neurosci* 2000;15:314–329.
 46. Goddard DR, Berry M, Kirvell SL, Butt AM. Fibroblast growth factor-2 inhibits myelin production by oligodendrocytes in vivo. *Mol Cell Neurosci* 2001;18:557–569.
 47. Patel JR, Klein RS. Mediators of oligodendrocyte differentiation during remyelination. *FEBS Lett* 2011;585:3730–3737.
 48. Furusho M, Dupree JL, Nave KA, Bansal R. Fibroblast growth factor receptor signaling in oligodendrocytes

- regulates myelin sheath thickness. *J Neurosci* 2012;32:6631–6641.
49. Frost GI. Recombinant human hyaluronidase (rHuPH20): an enabling platform for subcutaneous drug and fluid administration. *Expert Opin Drug Deliv* 2007;4:427–440.
 50. Huang Z, Zhao C, Chen Y, et al. Recombinant human hyaluronidase PH20 does not stimulate an acute inflammatory response and inhibits lipopolysaccharide-induced neutrophil recruitment in the air pouch model of inflammation. *J Immunol* 2014;192:5285–5295.
 51. Sunkin SM, Ng L, Lau C, et al. Allen Brain Atlas: an integrated spatio-temporal portal for exploring the central nervous system. *Nucleic Acids Res* 2013;41(Database issue):D996–D1008.
 52. Lein ES, Hawrylycz MJ, Ao N, et al. Genome-wide atlas of gene expression in the adult mouse brain. *Nature* 2007;445:168–176.
 53. Diez-Roux G, Banfi S, Sultan M, et al. A high-resolution anatomical atlas of the transcriptome in the mouse embryo. *PLoS Biol* 2011;9:e1000582.
 54. Hawrylycz MJ, Lein ES, Guillozet-Bongaarts AL, et al. An anatomically comprehensive atlas of the adult human brain transcriptome. *Nature* 2012;489:391–399.
 55. Wilhelm M, Schlegl J, Hahne H, et al. Mass-spectrometry-based draft of the human proteome. *Nature* 2014;509:582–587.
 56. Galtrey CM, Kwok JC, Carulli D, et al. Distribution and synthesis of extracellular matrix proteoglycans, hyaluronan, link proteins and tenascin-R in the rat spinal cord. *Eur J Neurosci* 2008;27:1373–1390.
 57. Wang H, Zhan Y, Xu L, et al. Use of suppression subtractive hybridization for differential gene expression in stroke: discovery of CD44 gene expression and localization in permanent focal stroke in rats. *Stroke* 2001;32:1020–1027.
 58. Bruckner G, Szeoke S, Pavlica S, et al. Axon initial segment ensheathed by extracellular matrix in perineuronal nets. *Neuroscience* 2006;138:365–375.
 59. Struve J, Maher PC, Li YQ, et al. Disruption of the hyaluronan-based extracellular matrix in spinal cord promotes astrocyte proliferation. *Glia* 2005;52:16–24.
 60. Suzuki K, Katzman R, Korey SR. Chemical studies on Alzheimer's disease. *J Neuropathol Exp Neurol* 1965;24:211–224.
 61. Jenkins HG, Bachelard HS. Developmental and age-related changes in rat brain glycosaminoglycans. *J Neurochem* 1988;51:1634–1640.
 62. Back SA, Kroenke CD, Sherman LS, et al. White matter lesions defined by diffusion tensor imaging in older adults. *Ann Neurol* 2011;70:465–476.
 63. Jenkins HG, Bachelard HS. Glycosaminoglycans in cortical autopsy samples from Alzheimer brain. *J Neurochem* 1988;51:1641–1645.
 64. Cargill R, Kohama SG, Struve J, et al. Astrocytes in aged nonhuman primate brain gray matter synthesize excess hyaluronan. *Neurobiol Aging* 2012;33:830.e813–830.e824.
 65. Carulli D, Rhodes KE, Fawcett JW. Upregulation of aggrecan, link protein 1, and hyaluronan synthases during formation of perineuronal nets in the rat cerebellum. *J Comp Neurol* 2007;501:83–94.
 66. Erickson M, Stern R. Chain gangs: new aspects of hyaluronan metabolism. *Biochem Res Int* 2012;2012:893947.
 67. Arranz AM, Perkins KL, Irie F, et al. Hyaluronan deficiency due to Has3 knock-out causes altered neuronal activity and seizures via reduction in brain extracellular space. *J Neurosci* 2014;34:6164–6176.

Supporting Information

Additional Supporting Information may be found online in the supporting information tab for this article:

Figure S1: Western Blot Analysis of Anti-rMuPH20 Antibodies. Lane M: molecular weight marker. Lanes 1–4: increasing amounts (25, 50, 100, and 200 ng) of the rMuPH20-FLAG protein. Panel A) blot probed with Ab1637 and B) blot probed with Ab2678.

Figure S2: Ab1637 polyclonal rabbit anti-murine PH20 testis labeling. Sections of testis from three mouse genotypes: wild type (A, D, G), *Spam1* knockout (B, E, H), *Hyal5* knockout (C, F, I) were labeled with a dilution of 2.5 $\mu\text{g}/\text{mL}$ of Ab1637 incubated overnight at 4°C. The antibody was either applied directly (A, B, C) or was preincubated with 400 $\mu\text{g}/\text{mL}$ of recombinant murine PH20 protein (D, E, F) or 400 $\mu\text{g}/\text{mL}$ of recombinant murine *Hyal5* protein (G, H, I) at ambient temperature for 90 min prior to immunolabeling. Tissue sections were counterstained with Gill's hematoxylin (Vector Laboratories). Results demonstrate that the Ab1637 anti-MuPH20 antibody cross-reacts with the highly homologous *Hyal5* enzyme.²⁷ Scale bar = 50 μm . Insert box scale bar = 200 μm .

Figure S3: Ab2678 polyclonal rabbit anti-murine PH20 testis labeling. Sections of testis from three mouse genotypes: wild type (A, D, G), *Spam1* knockout (B, E, H), *Hyal5* knockout (C, F, I) were labeled with a dilution of 2.5 $\mu\text{g}/\text{mL}$ of Ab2678 incubated for 30 min at ambient temperature. The antibody was either applied directly (A, B, C) or was preincubated with 400 $\mu\text{g}/\text{mL}$ of recombinant murine PH20 protein (D, E, F) or 400 $\mu\text{g}/\text{mL}$ of recombinant murine *Hyal5* protein (G, H, I) at ambient temperature for 90 min prior to immunolabeling. Tissue sections were counterstained with Gill's hematoxylin. Results demonstrate that the Ab2678 anti-MuPH20 antibody cross-reacts with the highly homologous *Hyal5* enzyme.²⁷ Scale bar = 50 μm . Insert box scale bar = 200 μm .

Figure S4: Comparative testis labeling of anti-*spam1* antibodies. Sections of testis from three mouse genotypes, wild type (A, B, C), *Spam1* knockout (D, E, F), and *Hyal5* knockout (G, H, I), were labeled with a dilution of two different rabbit polyclonal antibodies. Tissue sections (B, E, H) were labeled with Ab2678 anti-*spam1* (Halozyme Therapeutics, CA) diluted at 2.5 $\mu\text{g}/\text{mL}$ in TBS 10% normal goat serum for 30 min at ambient temperature. Tissue sections (C, F, I) were labeled with anti-*spam1*/PH20 (LS-C192906, LSBIO, WA) diluted at 1/500 in TBS 10% normal goat serum for 30 min at ambient temperature. Antibody labeling was revealed using a secondary antibody coupled with Vectastain ABC Elite (Vector Laboratories, Burlingame, CA) according to manufacturer's instructions. Tissue sections were counterstained with Gill's hematoxylin. Results demonstrated that the Ab2678 antibody generated better specificity than the rabbit polyclonal anti-*spam1*/PH20 antibody. Scale bar = 80 μm . Insert high magnification micrographs scale bar = 40 μm .

Figure S5: Comparative spinal cord labeling of anti-*spam1* antibodies. Sections of spinal cord from three mouse genotypes, wild type (A, B, C), *Spam1* knockout (D, E, F), and *Hyal5* knockout (G, H, I), were labeled with a dilution of two different rabbit polyclonal antibodies. Tissue sections (B, E, H) were labeled with Ab2678 anti-*spam1* (Halozyme Therapeutics, CA) diluted at 2.5 $\mu\text{g}/\text{mL}$ in TBS 10% normal goat serum for 30 min at ambient temperature. Tissue sections (C, F, I) were labeled with anti-*spam1*/PH20 (LS-C192906, LSBIO, WA) diluted at 1/500 in TBS 10% normal goat serum for 30 min at ambient temperature. Antibody labeling was revealed using a secondary antibody coupled with Vectastain ABC Elite (Vector Laboratories, Burlingame, CA) according to manufacturer's instructions. Tissue sections were counterstained with Gill's hematoxylin. Results demonstrated that the Ab2678 antibody generated better specificity than the rabbit polyclonal anti-*spam1*/PH20 antibody. Scale bar = 80 μm . Insert high magnification micrographs scale bar = 40 μm .

Figure S6: Comparative brain labeling of anti-*spam1* antibodies. Sections of brain from three mouse genotypes, wild type (A, B, C), *Spam1* knockout (D, E, F), and *Hyal5* knockout (G, H, I), were labeled with a dilution of two different rabbit polyclonal antibodies. Tissue sections (B, E, H) were labeled with Ab2678 anti-*spam1*

(Halozyme Therapeutics, CA) diluted at 2.5 $\mu\text{g}/\text{mL}$ in TBS 10% normal goat serum for 30 min at ambient temperature. Tissue sections (C, F, I) were labeled with anti-*spam1*/PH20 (LS-C192906, LSBIO, WA) diluted at 1/500 in TBS 10% normal goat serum for 30 min at ambient temperature. Antibody labeling was revealed using a secondary antibody coupled with Vectastain ABC Elite (Vector Laboratories, Burlingame, CA) according to manufacturer's instructions. Tissue sections were counterstained with Gill's hematoxylin. Results demonstrated that the Ab2678 antibody generated better specificity than the rabbit polyclonal anti-*spam1*/PH20 antibody. Scale bar = 80 μm . Insert high magnification micrographs scale bar = 40 μm .

Figure S7: HA fragments generated by PH20 did not inhibit OPC differentiation. (A) Rat OPCs were incubated with T3 hormone (200 ng/mL, Sigma-Aldrich) and 40 $\mu\text{g}/\text{mL}$ of bovine testicular hyaluronidase BTH IV-S (Hyal type IV-S (SLBC1033V), Sigma-Aldrich), BTH IV-S (Hyal type IV-S (SLBD1402V), Sigma-Aldrich), recombinant human PH20 (rHuPH20), and recombinant murine PH20 (rMuPH20: 340,000 U/mg) for 4 days. Neither rMuPH20 nor rHuPH20 enzymes inhibited OPC differentiation. In contrast, both samples of BTH IV-S significantly inhibited OPC differentiation. (B) High-molecular-weight (HMW) (1.5MDa), endotoxin-free hyaluronan was incubated with the indicated PH20 preparations for 60 min at 37°C. After incubation, each solution was heated to 95°C for 60 min to inactivate the enzymes. The resulting HMW HA digestion products were resolved by a 4–20% gradient polyacrylamide gel electrophoresis and visualized with 0.005% Stains-All (Sigma-Aldrich) in 50% ethanol to demonstrate enzymatic activity. (C) Rat OPCs were incubated for 4 days with T3 hormone (200 ng/mL, Sigma-Aldrich) and 50 $\mu\text{g}/\text{mL}$ of high-molecular-weight (HMW) HA or HA fragments generated by the coincubation of HMW HA with different hyaluronidases (rHuPH20, rMuPH20, and BTHs) described in panel B. None of the enzymatically generated HA fragment pools significantly inhibited OPC differentiation. In contrast, incubation of HMW HA with the cells resulted in a statistically significant inhibition of OPC differentiation. For (A) and (C), the positive control was generated by exposing OPCs to T3 hormone alone. Statistical significance was computed by one-way ANOVA.